




Article

Geometric Structure behind Duality and Manifestation of Self-Duality from Electrical Circuits to Metamaterials

Yosuke Nakata ^{1,*}, Yoshiro Urade ² and Toshihiro Nakanishi ³

¹ Research Center for Advanced Science and Technology, The University of Tokyo, Meguro-ku, Tokyo 153-8904, Japan

² Center for Emergent Matter Science, RIKEN, Wako, Saitama 351-0198, Japan; yoshiro.urade@riken.jp

³ Department of Electronic Science and Engineering, Kyoto University, Kyoto 615-8510, Japan; t-naka@kuee.kyoto-u.ac.jp

* Correspondence: nakata@ee.es.osaka-u.ac.jp

† Current address: Graduate School of Engineering Science, Osaka University, Toyonaka, Osaka 560-8531, Japan.

Received: 31 August 2019; Accepted: 14 October 2019; Published: 28 October 2019



Abstract: In electromagnetic systems, duality is manifested in various forms: circuit, Keller–Dykhne, electromagnetic, and Babinet dualities. These dualities have been developed individually in different research fields and frequency regimes, leading to a lack of unified perspective. In this paper, we establish a unified view of these dualities in electromagnetic systems. The underlying geometrical structures behind the dualities are elucidated by using concepts from algebraic topology and differential geometry. Moreover, we show that seemingly disparate phenomena, such as frequency-independent effective response, zero backscattering, and critical response, can be considered to be emergent phenomena of self-duality.

Keywords: duality; self-duality; Poincaré duality; circuit duality; Keller–Dykhne duality; electromagnetic duality; Babinet’s principle; constant-resistance circuit; zero backscattering; critical response; self-complementary antenna; metamaterials; metasurfaces

1. Introduction

Duality is an indispensable concept in mathematics, physics, and engineering. It relates two seemingly different systems in a nontrivial manner and facilitates deeper insight into the underlying structures behind the relevant physical theories. A duality transformation converts an object to its dual counterpart. Performing duality transformations twice brings a system back to its original state. Advantageously, duality transformation can sometimes convert a difficult problem into a more tractable one. Moreover, if a system is dual to itself, namely self-dual, some special characteristics could be expected. To name a few, self-duality characterizes a critical probability and temperature for percolation on graphs [1,2] and two-dimensional Ising models [3], respectively.

For electromagnetic systems, duality appears in various forms, such as dual circuits [4,5], Keller–Dykhne duality [6–8], electromagnetic duality [9–11], input–impedance duality for antennas [12,13], and Babinet’s principle [14–26]. These dualities have been individually developed in various research fields such as electrical engineering, radio-frequency engineering, and photonics because the relevant frequency spectra broadly range from direct-current to the optical regime. Despite the long history of dualities in electromagnetic systems, they have not been sufficiently discussed from a unified perspective. In particular, universal geometrical structures behind the dualities are still mathematically unclear in electromagnetic systems.

Recently, engineered artificial composites called metamaterials have been attracting much attention due to their exotic electromagnetic properties [27]. In particular, two-dimensional metamaterials are called metasurfaces and are intensively studied as ultrathin functional devices [28–30]. The operating frequency of metamaterials has been extended from the microwave to the optical band, and versatile design principles over extensively wide frequency spectra are in high demand. For example, circuit designs and nano-optics were integrated to establish a universal strategy to design metamaterials [31]. Over the past few decades, duality has been assuming an important role in the research and development of metamaterials. To name a few such cases, duality has been leveraged to design complementary metasurfaces [32–35], self-complementary metasurfaces [36–42], critical metasurfaces [43–52], maximally chiral metamaterials [53], and self-dual metamaterials with zero backscattering [54] or helicity conservation [55–57]. In such situations, the extensive target frequencies of metamaterials require a comprehensive understanding of duality in a unified manner.

In this paper, we establish a unified perspective which synthesizes dualities appearing in electromagnetic systems. The underlying geometrical structures hidden behind dualities are uncovered through Poincaré duality between circuit theory to optics. To this end, we introduce inner and outer orientations of geometrical objects. We stress the importance of these two different kinds of orientations because it is sometimes overlooked in primary electromagnetism. The correspondence relationship among various dualities in electromagnetic systems is thoroughly discussed. Moreover, we comprehensively show that self-duality manifests as frequency-independent effective response, zero backscattering, and criticality in electromagnetic systems. As a whole, we attempted to keep the paper pictorial as much as possible in order to easily grasp the important concepts for duality.

In Section 2, we start with discussions of electrical circuits. Although electrical circuits are simplified and idealized systems, they include the essence of duality. To clearly see duality in circuit theory, we provide an algebraic-topological framework for electrical circuits. Based on the established framework, we strictly formulate circuit duality through Poincaré duality. Furthermore, we explain that the effective response of a self-dual circuit is automatically derived from its self-duality. In Section 3, we discuss zero backscattering for waves in self-dual circuits in terms of impedance matching. Section 4 generalizes circuit duality to Keller–Dykhne duality for a continuous two-dimensional resistive sheet. We show that critical behavior can appear for a self-dual sheet. To extract the essence of the duality in continuous systems, differential forms are utilized. We see that Keller–Dykhne duality exactly corresponds to circuit duality through discretization. In Section 5, we introduce electromagnetic duality to Maxwell’s electromagnetic theory. Electromagnetic duality in a four-dimensional spacetime has a similar structure to Keller–Dykhne duality in a two-dimensional plane. Section 6 introduces duality for wave radiation and scattering by a two-dimensional sheet. Combining electromagnetic duality and mirror symmetry of the sheet, we establish Babinet duality. Babinet duality induces the critical response of a metallic checkerboard-like sheet. Finally, Section 7 summarizes the unified perspective for dualities appearing in electromagnetic systems and gives a conclusion.

2. Circuit Theory

In this section, we establish a comprehensive formulation of circuit theory based on algebraic topology. Within the proposed framework that makes use of Poincaré duality, we unveil the geometrical structure of circuit duality. Next, we discuss the resultant duality in effective response and show that a specific response is automatically guaranteed under self-duality. Compared to the previous algebraic topological formulation of the circuit theory [58–60], we clarify the importance of inner and outer orientations of geometrical objects for circuit duality. Our approach gives a succinct mathematical description of circuit duality, and an amalgamation of circuit theory and algebraic topology yields various benefits in this interdisciplinary area.

2.1. Duality between Current and Voltage

■ Circuits as Graphs

A circuit is considered as a network of interconnected components. The interconnection relation can be represented by a graph $\mathcal{G} = (\mathcal{N}, \mathcal{E})$ with a set $\mathcal{N} = \{n_i | i = 1, 2, \dots, |\mathcal{N}|\}$ expressing the totality of nodes and a set $\mathcal{E} = \{e_i | i = 1, 2, \dots, |\mathcal{E}|\}$ representing the totality of directed edges (an ordered 2-element subset of \mathcal{N}), where $|\mathcal{S}|$ is the number of elements of a set \mathcal{S} . Elements in \mathcal{N} and \mathcal{E} are called 0- and 1-cells, respectively. Circuit elements such as voltage sources or resistors are placed along the graph edges. In this section, we mainly focus on circuits with resistors, voltage, and current sources. Figure 1 shows an example of a circuit and the corresponding graph.

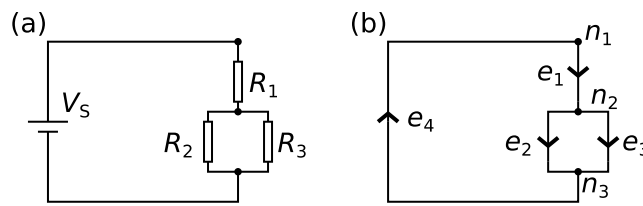


Figure 1. Example of (a) a circuit and (b) its corresponding graph, which represents the circuit interconnection.

■ Chains

Consider a current distribution with I^i flowing along each edge $e_i \in \mathcal{E}$. Here, e_i is directed and I^i flows in the direction of e_i . A negative I^i represents a current flow in the reverse direction of e_i . This current distribution can be represented by a formal sum $I = \sum_{i=1}^{|\mathcal{E}|} I^i e_i$, where \mathcal{E} generates a vector space over real numbers \mathbb{R} . In a strict sense, we should consider $\mathbb{R}A := \{sA | s \in \mathbb{R}\}$ with the unit of ampere A instead of \mathbb{R} for a current distribution, but we omitted the unit to avoid notation complexity. A vector spanned by elements in \mathcal{E} is called a 1-chain. The vector space composed of all 1-chains is denoted by C_1 . Similarly, we can define a 0-chain as $\sum_{i=1}^{|\mathcal{N}|} q^i n_i$ with $q^i \in \mathbb{R}$, and introduce a vector space C_0 over \mathbb{R} as the totality of 0-chains.

■ Boundary Operator

Now, we extract the connection information regarding \mathcal{G} . Consider an edge e directing from a node n_1 to n_2 . As shown in Figure 2, the boundary of e is given by $\partial e = n_2 - n_1$. Extending the definition linearly, we can introduce a linear boundary operator $\partial : C_1 \rightarrow C_0$. The matrix representation of ∂ is denoted by Δ^i_j , called the incidence matrix. For the previous example in Figure 1b, we obtain the following matrix representation of ∂ :

$$\partial[e_1 \ e_2 \ e_3 \ e_4] := [\partial e_1 \ \partial e_2 \ \partial e_3 \ \partial e_4] = [n_1 \ n_2 \ n_3] \Delta \tag{1}$$

with

$$\Delta = [\Delta^i_j] = \begin{bmatrix} -1 & 0 & 0 & 1 \\ 1 & -1 & -1 & 0 \\ 0 & 1 & 1 & -1 \end{bmatrix}. \tag{2}$$

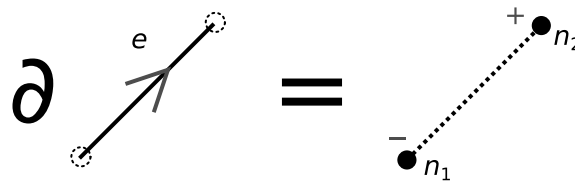


Figure 2. Action of the boundary operator. Here, we have $\partial e = n_2 - n_1$.

■ Kirchhoff's Current Law

To understand the physical meaning of ∂ , we consider ∂I for a current distribution $I \in C_1$. The coefficient of ∂I for $n \in \mathcal{N}$ represents the net inflow of the current: the current inflow to n minus the current outflow from n . Therefore, the boundary operator can be used to express Kirchhoff's current law (KCL), which states that net current inflows at each node are zero. KCL restricts current distribution to a linear subspace $Z_1 = \ker \partial = \{c \in C_1 | \partial c = 0\}$. For Equation (2), we have $\text{rank } \Delta = 2$, and $\dim Z_1 = \dim C_1 - \text{rank } \Delta = 2$ from the rank-nullity theorem [61]. The basis of Z_1 is given by $\{m_1 = e_1 + e_2 + e_4, m_2 = e_2 - e_3\}$. Here, m_1 and m_2 are closed loops called *meshes*. Generally, we can construct a basis of Z_1 with meshes [60].

■ Cochains

Next, we represent a voltage distribution in geometric terms. For a finite-dimensional vector space U , we can define its dual space $U^* = \{\alpha : U \rightarrow \mathbb{R}\}$, where α is a linear map and U^* is a vector space with $\dim U^* = \dim U$. An element $\alpha \in U^*$ can be interpreted as an apparatus which measures a vector $u \in U$ and yields $\alpha(u)$. For a basis $\{u_1, u_2, \dots, u_m\}$ in U , we can define a dual basis $\{u^1, u^2, \dots, u^m\}$ in U^* satisfying $u^i(u_j) = \delta_j^i$, where the Kronecker delta δ_j^i is 1 if $i = j$; otherwise, 0. For a vector $v = \sum_{i=1}^m v^i u_i \in U$ with $v^i \in \mathbb{R}$, u^i extracts the component with respect to u_i as $u^i(v) = v^i$.

Along an edge, we can calculate power consumption as a real scalar equal to the voltage multiplied by the current. The total power consumption in the circuit is the sum of power consumption over all edges (power generation is represented by negative power consumption). Therefore, a voltage distribution is considered as $V \in C^1 = (C_1)^*$ yielding total power $V(I)$ for $I \in C_1$. An element in C^1 is called a *1-cochain*. In C^1 , we have a dual basis $\{e^i | i = 1, 2, \dots, |\mathcal{E}|\}$. Then, we can express $V(I) = \sum_{i=1}^{|\mathcal{E}|} V_i I^i$ for $V = \sum_{i=1}^{|\mathcal{E}|} V_i e^i$ and $I = \sum_{i=1}^{|\mathcal{E}|} I^i e_i$. We also write $V(I)$ as $\int_I V$ to stress the analogy to the theory of continuous fields. A 0-cochain $\varphi \in C^0 = (C_0)^*$ also acts for a 0-chain $b \in C_0$ as $\int_b \varphi = \varphi(b)$.

■ Kirchhoff's Voltage Law

Now, we reframe Kirchhoff's voltage law (KVL) in our geometric approach. KVL states that the sum of voltages along any loop must be zero. Then, a voltage distribution $V \in C^1$ must satisfy $\int_I V = 0$ for all $I \in Z_1$ (also known as Tellegen's theorem) because I is generated from mesh currents. To concisely express KVL, we define a null space $(U')^\perp$ for a linear subspace U' in U as $(U')^\perp = \{\alpha \in U^* | \alpha(u) = 0 \text{ for all } u \in U'\}$. The dimension of the null space is given by $\dim(U')^\perp = \dim U - \dim U'$. The relation between U' and $(U')^\perp$ is schematically depicted in Figure 3. By using the concept of a null space, KVL is clearly rewritten to restrict voltage distribution to $(Z_1)^\perp$.

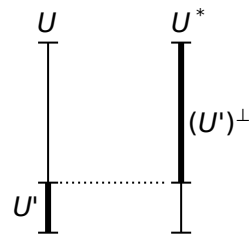


Figure 3. Relation between U' and $(U')^\perp$.

■ Dual Operators

Next, we want to define a dual boundary operator for ∂ . Let U and W be finite-dimensional vector spaces, and consider a linear map $f : U \rightarrow W$. Then, a dual map $f^* : W^* \rightarrow U^*$ is defined as $[f^*(\alpha)](u) := \alpha[f(u)]$ for $\alpha \in W^*$ and all $u \in U$. Let $\{u_1, u_2, \dots, u_l\}$ and $\{w_1, w_2, \dots, w_m\}$ be the bases of U and W , respectively. We have $f^*(w^i) = \sum_{j=1}^l [f^*(w^i)](u_j) u_j = \sum_{j=1}^l w^i[f(u_j)] u_j = \sum_{j=1}^l u_j M^i_j$ with the matrix representation of f as $M^i_j = w^i[f(u_j)]$. This shows that the matrix representation of the dual map is the transpose of the matrix representation of the original map. Using the concept of the dual map, we can define a coboundary operator $d = \partial^*$ to satisfy $\int_{\partial c} \varphi = \int_c d\varphi$ for all $c \in C_1$ and $\varphi \in C^0 = (C_0)^*$. For a dual basis $\{n^i\} \subset C^0$ obtained from 0-cells $\mathcal{N} = \{n_i\}$, we have $dn^i = \sum_{j=1}^{|\mathcal{E}|} e^j \Delta^i_j$ with the incidence matrix Δ^i_j . For the example of Figure 1b, we have

$$d[n^1 \ n^2 \ n^3] := [dn^1 \ dn^2 \ dn^3] = [e^1 \ e^2 \ e^3 \ e^4] \begin{bmatrix} -1 & 1 & 0 \\ 0 & -1 & 1 \\ 0 & -1 & 1 \\ 1 & 0 & -1 \end{bmatrix}. \tag{3}$$

■ Potential and Kirchhoff’s Voltage Law

Finally, we discuss a relation between KVL and a potential. KVL was formulated to state that the voltage drop along any loop is zero, but how is this statement related to the existence of a potential? To see this, we start from a general statement. Consider a linear map $f : U \rightarrow W$. The image and kernel of linear maps f and f^* are related through $(\ker f)^\perp = \text{im } f^*$ and $(\text{im } f)^\perp = \ker f^*$ [61]. The proof of the first statement is as follows. First, $(\ker f)^\perp \supset \text{im } f^*$ holds because we have $f^*(\beta)(u) = \beta(f(u)) = 0$ for all $u \in \ker f$ with $\beta \in W^*$. Second, $\dim(\ker f)^\perp = \dim U - \dim \ker f = \text{rank } f = \text{rank } f^*$ holds due to the rank–nullity theorem. Then, we obtain $(\ker f)^\perp = \text{im } f^*$. A similar proof is applied for the second statement. Now, we come back to circuit theory and define $B^1 = \text{im } d \subset C^1$. From $(\ker \partial)^\perp = \text{im } d$, we obtain $(Z_1)^\perp = B^1$. This means that there is a potential $\varphi \in C^0$ which satisfies $V = -d\varphi$ for a voltage distribution V .

■ Summary of Circuit Equations

The discussions so far show the duality between KCL and KVL. These results are summarized in Figure 4. Importantly, the degree of freedom for currents and voltages constrained by KCL and KVL is given by $\dim Z_1 + \dim B^1 = \dim C_1$. On the other hand, a circuit element along each edge gives the relation between the current and voltage on the edges, and we have $\dim C_1$ equations with respect to all the circuit elements. Therefore, the current and voltage distributions are unambiguously determined.

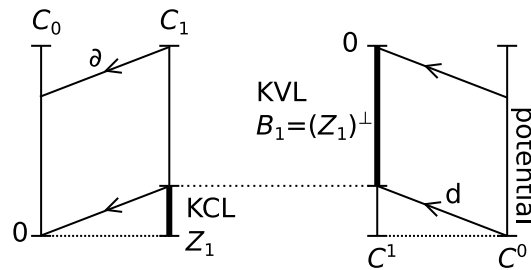


Figure 4. Duality between Kirchhoff's current and voltage laws.

2.2. Planar Graph as Cellular Paving

Consider the series and parallel resistors shown in Figure 5. Series resistors R_1 and R_2 have the composite resistance $R = R_1 + R_2$. On the other hand, parallel resistors R'_1 and R'_2 have the total resistance R' , satisfying $1/R' = 1/R'_1 + 1/R'_2$. We can clearly see the duality between resistance and conductance (given by an inverse relationship) for series and parallel resistances. This duality universally holds in more general situations, as we show in Section 2.5. In this subsection, we set up a fundamental geometric structure to establish circuit duality.

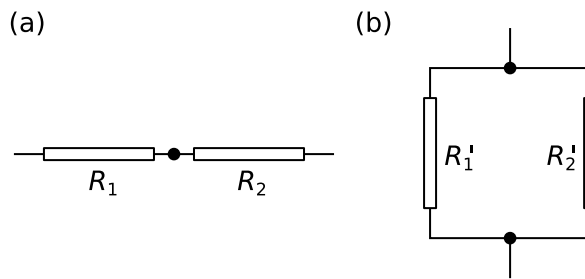


Figure 5. (a) series and (b) parallel resistors with composite resistances R and R' , respectively. The duality between resistance and conductance appears as $R = R_1 + R_2$ and $1/R' = 1/R'_1 + 1/R'_2$.

■ 2-Chains in Planar Graphs

The graph shown in Figure 1b is *planar*, i.e., its edges intersect only at their nodes. For a planar graph, we can define faces. In Figure 6, we show directed faces $\mathcal{F} = \{f_1, f_2, f_3\}$, where the internal direction of each face is represented by the directed circle. Elements of \mathcal{F} are called 2-cells. Note that we include the unbounded face f_3 outside the circuit. The area of face f_3 can be finite if we consider the planar graph to be on a sphere. The vector space generated by \mathcal{F} is denoted by C_2 . It is natural to define a boundary operator $\partial : C_2 \rightarrow C_1$, such that $e^j(\partial f_i) = 1$ [$e^j(\partial f_i) = -1$] if $e_j \in \mathcal{E}$ is included in f in the same [opposite] direction; otherwise, $e^j(\partial f_i) = 0$. For Figure 6, we have

$$\partial[f_1 \ f_2 \ f_3] := [\partial f_1 \ \partial f_2 \ \partial f_3] = [e_1 \ e_2 \ e_3 \ e_4] \begin{bmatrix} 1 & 0 & 1 \\ 1 & -1 & 0 \\ 0 & 1 & 1 \\ 1 & 0 & 1 \end{bmatrix}. \tag{4}$$

Note that $\partial \circ \partial = 0$ holds, i.e., the boundary of a cell boundary is empty.

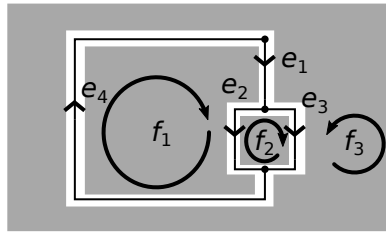


Figure 6. Faces in a planar circuit.

■ Cellular Paving

In the previous examples, cells fully paved the two-dimensional plane without any gap. Such a paving is often called a mesh in finite element analysis. Naturally, a p -cell is defined as a p -dimensional directed face, which is extended from a 0-cell (point), 1-cell (edge), and 2-cell (face). Cellular paving with the cells can be rigorously formulated in higher-dimensional spaces. The boundary of each element is represented by a combination of lower-dimensional cells. Strictly speaking, a cellular paving of some region R in a manifold is a finite set of open directed p -cells such that (i) two distinct cells do not intersect, (ii) the union of all cells is R , and (iii) if the closures of two cells c and c' meet, their intersection is the closure of a unique cell c'' [62]. However, we only need to grasp the concept of cellular paving with an intuitive sense.

For a cellular paving \mathcal{K} in an m -dimensional region, we can define $C_i(\mathcal{K})$ ($i = 0, 1, \dots, m$) generated from i -cells with a boundary operator $\partial : C_p(\mathcal{K}) \rightarrow C_{p-1}(\mathcal{K})$ satisfying $\partial \circ \partial = 0$. Following a similar treatment for graphs, $Z_p(\mathcal{K}) = \ker(\partial : C_p(\mathcal{K}) \rightarrow C_{p-1}(\mathcal{K}))$ and $B_p(\mathcal{K}) = \text{im}(\partial : C_{p+1}(\mathcal{K}) \rightarrow C_p(\mathcal{K}))$ are defined. Next, we consider a dual space $C^p(\mathcal{K}) = (C_p(\mathcal{K}))^*$. As dual counterparts of $Z_p(\mathcal{K})$ and $B_p(\mathcal{K})$, we can define $Z^p(\mathcal{K}) = \ker(d : C^p(\mathcal{K}) \rightarrow C^{p+1}(\mathcal{K}))$ and $B^p(\mathcal{K}) = \text{im}(d : C^{p-1}(\mathcal{K}) \rightarrow C^p(\mathcal{K}))$. To extract topological characteristics, homology and cohomology groups are defined as $H_p(\mathcal{K}) = Z_p(\mathcal{K})/B_p(\mathcal{K})$ and $H^p(\mathcal{K}) = Z^p(\mathcal{K})/B^p(\mathcal{K})$, respectively. It is known that $\dim H_p(\mathcal{K})$ and $\dim H^p(\mathcal{K})$ do not depend on specific cellular paving, but only on the original m -dimensional region.

2.3. Inner and Outer Orientations

■ Intuitive Explanation of Inner and Outer Orientations

Thus far, cells were assumed to be (internally) oriented. In this subsection, we clarify the definition of orientation and provide a deeper explanation that is crucial for understanding the circuit duality. First, one can intuitively grasp two types of orientation defined for a surface in a three-dimensional space. In Figure 7a, the surface is internally oriented, where “internally” means that the orientation is defined through the internal coordinates of the surface, regardless of whether or not the surface is embedded in the three-dimensional space. On the other hand, we could consider an outer orientation of the surface as the normal-vector field as shown in Figure 7b. Outer orientation refers to the transverse direction of the surface and involves ambient space. To discuss how much fluid traverses the surface, we do not use an inner-oriented surface, but an outer-oriented one. These two types of orientation are strictly defined below and are important to express various physical quantities.

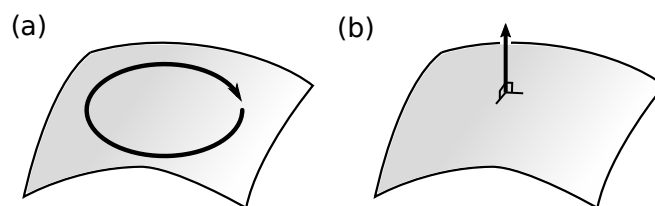


Figure 7. Two types of orientation: (a) inner and (b) outer orientation of a surface in a three-dimensional space.

■ Inner Orientation of Vector Space and Cell

As a starting point, we define an inner orientation of a vector space U . Consider two ordered bases (e_1, e_2, \dots, e_m) and $(e'_1, e'_2, \dots, e'_m)$ in U . A basis transformation is represented by $e'_i = \sum_{j=1}^m e_j P^j_i$. When $\det P > 0$, the direction associated with (e_1, e_2, \dots, e_m) is considered to be the same as that with $(e'_1, e'_2, \dots, e'_m)$; otherwise, their directions are different. Then, bases are classified as two different equivalence classes. We can choose one specific class to be positive orientation. If a vector space U has such a positive orientation, U is called inner-oriented. Generally, a tangent space $T_p M$ is a p -dimensional vector space composed of tangent vectors at a point P on a p -dimensional surface (manifold) (Figure 8a). If tangent spaces on a p -cell are continuously oriented, it is called inner-oriented. See a schematic picture shown in Figure 8b.

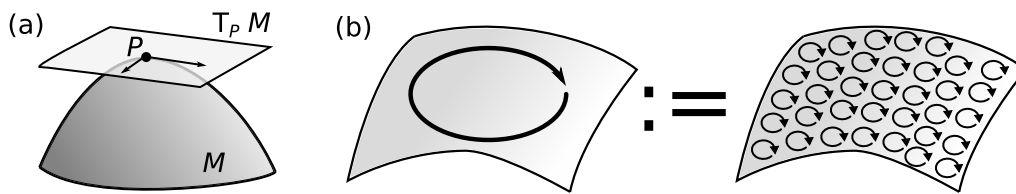


Figure 8. (a) tangent space $T_p M$ at a point P on a surface M ; (b) inner-oriented 2-cell with continuously oriented tangent spaces.

■ Outer Orientation of Vector Space and Cell

Next, we introduce an outer orientation. Consider a linear subspace W in a vector space U . When we choose an orientation of the quotient vector space U/W , we say that W is *outer-oriented*. The outer orientation is naturally extended to a p -cell S in an m -dimensional manifold M . Here, M is a total space including S and called ambient space. Because of $T_p S \subset T_p M$, we can consider $T_p M/T_p S$ as a vector space whose (nonzero) elements are considered to be transverse to $T_p S$. If a p -cell has continuous orientation of $T_p M/T_p S$ for all $P \in S$, the cell is called outer-oriented. An example of an outer-oriented 2-cell is shown in Figure 9.

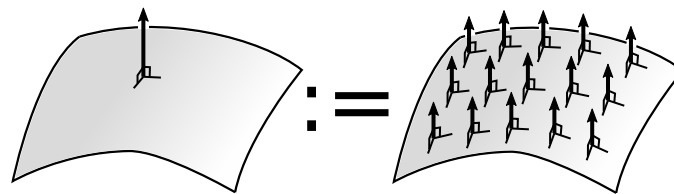


Figure 9. Outer-oriented 2-cell S in a three-dimensional space is continuously outer-oriented in all tangent spaces.

For a planar paving, we summarize all types of cells in Figure 10. An outer-oriented 0-cell is best suited to represent a rotation around a point in the two-dimensional plane. Fluid flow transverse to an edge is also represented by an outer-oriented 1-cell.

	inner-oriented	outer-oriented	
0			point
1			edge
2			face

Figure 10. Inner- and outer-oriented cells in a two-dimensional plane.

■ Inner-Orientation Representation for Outer Orientation

Outer orientation can be represented by two inner orientations depending on the orientation of ambient space. Let us see this representation in an example in a two-dimensional plane. Consider an outer-oriented edge in a planar graph. With a given orientation of the plane (two-dimensional Euclid space \mathbb{E}_2), we can convert the outer orientation into an inner one as shown in Figure 11. The inner orientation is induced by rotating the outer orientation by 90° , where the rotational direction is determined by the ambient-space orientation. Importantly, the inner direction is reversed when we choose the opposite ambient-space orientation. Thus, an outer-oriented cell \check{s} can be represented by two different inner-oriented cells as $\check{s} = \{\check{s}_o | o = \circlearrowleft, \circlearrowright\}$ with $\check{s}_{\circlearrowleft} = -\check{s}_{\circlearrowright}$. The above intuitive discussion can be generalized in other dimensional spaces as shown in Appendix A.

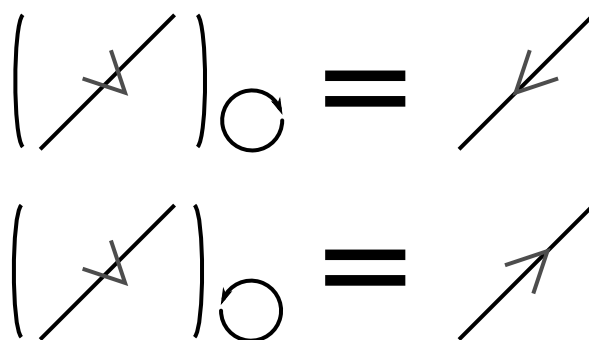


Figure 11. Inner-oriented components of an outer-oriented edge in a two-dimensional plane. The plane orientations are given by the subscripts ($\circlearrowleft, \circlearrowright$).

■ Outer-Orientation Representation for Inner Orientation

The previous discussions on orientations are based on representations of an outer-oriented cell by inner-oriented cells. We would like to remark on a dual perspective: an inner-oriented cell can be represented by outer-oriented cells. This perspective is indicated in Figure 12. To obtain an outer orientation, the inner orientation of the edge is rotated by 90° in the reverse direction of a given orientation of the plane.

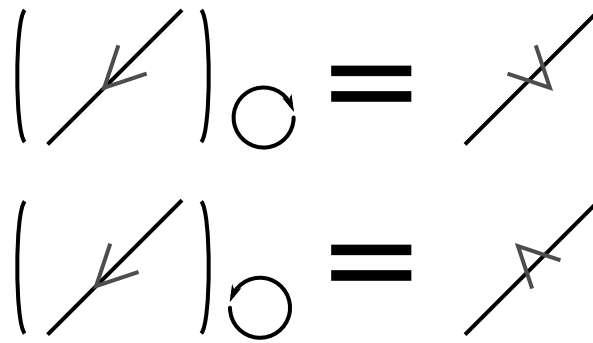


Figure 12. Outer-oriented components of an inner-oriented edge in a two-dimensional plane.

■ Operation for Outer-Oriented Chains and Cochains

Next, consider a cellular paving \check{K} with outer-oriented cells. We can define a vector space $C_p(\check{K})$ generated from p -cells in \check{K} . Using the representation of an outer-oriented cell by inner-oriented cells, we can define $\partial : C_p(\check{K}) \rightarrow C_{p-1}(\check{K})$ so that ∂ individually acts for each inner-oriented component. For example, an inner-oriented component of the boundary of an outer-oriented 1-cell in a plane is depicted in Figure 13. The boundary operations for outer-oriented cells in a two-dimensional plane are summarized in Figure 14.

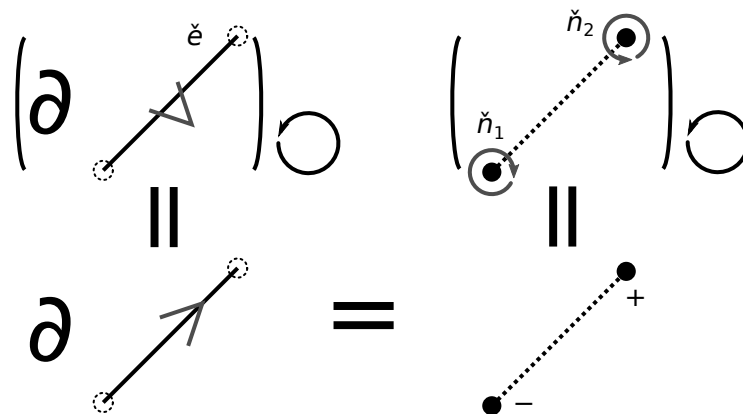


Figure 13. Boundary operation for an outer-oriented 1-cell in a two-dimensional plane is defined through the inner-oriented component.

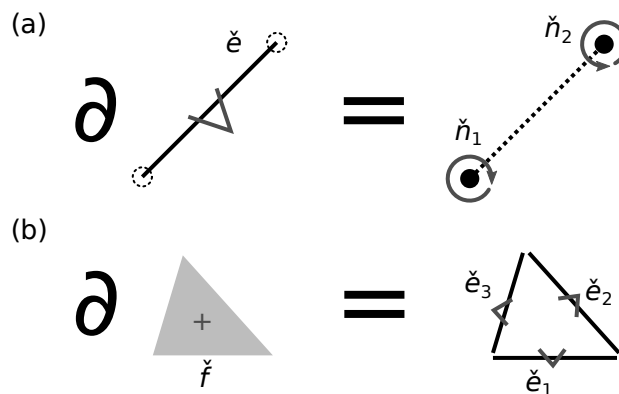


Figure 14. Boundary operation for an outer-oriented (a) edge and (b) face in a two-dimensional plane.

As a dual counterpart of $C_p(\check{K})$, the dual space $C^p(\check{K}) = (C_p(\check{K}))^*$ is defined by applying the general theory for linear spaces. An outer-oriented cochain in $C^p(\check{K})$ is also represented by two inner-oriented cochains and the coboundary operator d for outer-oriented cochains is naturally defined.

2.4. Essence of Poincaré Duality

■ Dual Paving

For a cellular paving \mathcal{K} with inner-oriented cells, we can compose a dual cellular paving \mathcal{K}^* with outer-oriented cells. Here, we focus on ambient space of a two-dimensional plane to introduce the concept. As shown in Figure 15a, each face f_i in \mathcal{K} is converted to an outer-oriented point \check{n}_i in \mathcal{K}^* . Each edge e_j in \mathcal{K} is also replaced with an outer-oriented edge \check{e}_j in \mathcal{K}^* transverse to the original edge. The obtained edge is connected to a point in \mathcal{K}^* , if the original edge is included in the original face. Furthermore, each point n_j in \mathcal{K} is converted to a face \check{f}_j in \mathcal{K}^* as shown in Figure 15b. The face is adjacent to an edge in \mathcal{K}^* , if the original point is connected to the original edge. Under this composition, the orientation of each cell is naturally inherited from the original cell to the dual cell.

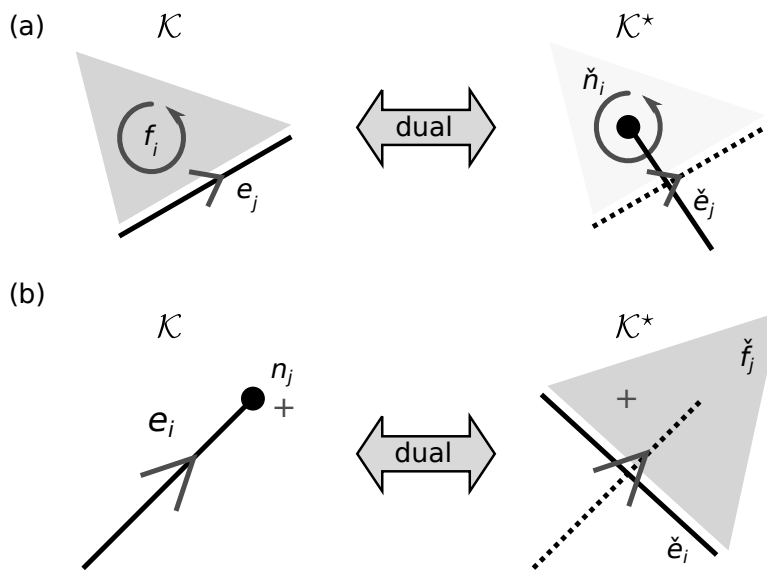


Figure 15. Correspondence between a cellular paving \mathcal{K} and its dual paving \mathcal{K}^* . (a) a face f_i in $\mathcal{K} \leftrightarrow$ a point \check{n}_i in \mathcal{K}^* ; (b) a point n_j in $\mathcal{K} \leftrightarrow$ a face \check{f}_j in \mathcal{K}^* . In both figures, an edge e_j in \mathcal{K} corresponds to an edge \check{e}_j in \mathcal{K}^* .

Let us explicitly see this composition in the previous example, where the original cellular paving is shown again in Figure 16a. By applying the above procedure for \mathcal{K} shown in Figure 16a, we obtain the dual paving \mathcal{K}^* as shown in Figure 16b.

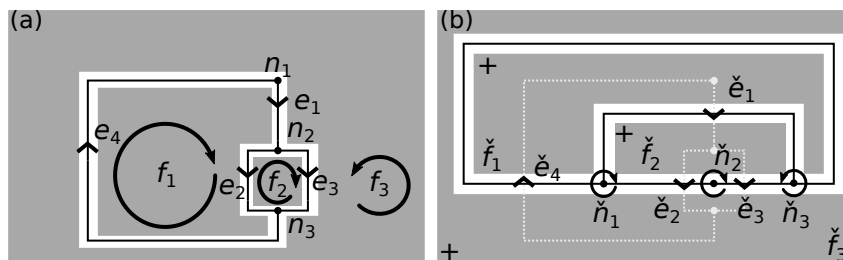


Figure 16. (a) cellular paving and (b) its dual paving.

■ Poincaré Duality

For this dual paving, we have the following matrix representations of ∂ :

$$\partial[\check{f}_1 \check{f}_2 \check{f}_3] = [\check{e}_1 \check{e}_2 \check{e}_3 \check{e}_4] \begin{bmatrix} 1 & -1 & 0 \\ 0 & 1 & -1 \\ 0 & 1 & -1 \\ -1 & 0 & 1 \end{bmatrix}, \quad (5)$$

$$\partial[\check{e}_1 \check{e}_2 \check{e}_3 \check{e}_4] = [\check{n}_1 \check{n}_2 \check{n}_3] \begin{bmatrix} 1 & 1 & 0 & 1 \\ 0 & -1 & 1 & 0 \\ 1 & 0 & 1 & 1 \end{bmatrix}. \quad (6)$$

Comparing Equations (5) and (6) with Equations (1) and (4), we have

$$[\partial : C_1(\mathcal{K}) \rightarrow C_0(\mathcal{K})] = -[\partial : C_2(\mathcal{K}^*) \rightarrow C_1(\mathcal{K}^*)]^T, \quad (7)$$

$$[\partial : C_2(\mathcal{K}) \rightarrow C_1(\mathcal{K})] = [\partial : C_1(\mathcal{K}^*) \rightarrow C_0(\mathcal{K}^*)]^T, \quad (8)$$

where the square brackets indicate matrix representation. The above relations $n^j(\partial e_i) = -\check{e}^i(\partial \check{f}_j)$ and $e^j(\partial f_i) = \check{n}^i(\partial \check{e}_j)$ hold from Figure 15. These relations universally hold even in a higher-dimensional space. Recalling $[d : C^p(\mathcal{K}) \rightarrow C^{p+1}(\mathcal{K})] = [\partial : C_{p+1}(\mathcal{K}) \rightarrow C_p(\mathcal{K})]^T$, we obtain the following commutative diagram:

$$\begin{array}{ccccc} C_2(\mathcal{K}) & \xrightarrow{\partial} & C_1(\mathcal{K}) & \xrightarrow{\partial} & C_0(\mathcal{K}) \\ \downarrow \star_2 & & \downarrow \star_1 & & \downarrow \star_0 \\ C^0(\mathcal{K}^*) & \xrightarrow{d} & C^1(\mathcal{K}^*) & \xrightarrow{-d} & C^2(\mathcal{K}^*) \end{array} \quad (9)$$

Here, we have isomorphisms $\star_p : C_p(\mathcal{K}) \rightarrow C^{m-p}(\mathcal{K}^*)$ with $m = 2$, where $\star_0 : n_i \mapsto \check{f}^i$, $\star_1 : e_i \mapsto \check{e}^i$, and $\star_2 : f_i \mapsto \check{n}^i$. The dual counterpart of Equation (9) is given by

$$\begin{array}{ccccc} C^2(\mathcal{K}) & \xleftarrow{d} & C^1(\mathcal{K}) & \xleftarrow{d} & C^0(\mathcal{K}) \\ \uparrow \star^2 & & \uparrow \star^1 & & \uparrow \star^0 \\ C_0(\mathcal{K}^*) & \xleftarrow{\partial} & C_1(\mathcal{K}^*) & \xleftarrow{-\partial} & C_2(\mathcal{K}^*) \end{array} \quad (10)$$

with $\star^i = (\star_i)^*$ using the dual map $(\star_i)^*$ of \star_i . These correspondences naturally hold in higher-dimensional spaces and lead to Poincaré duality: $H_p(M) \cong H^{m-p}(M)$ for a compact orientable m -dimensional manifold M [63].

2.5. Dual Circuits

■ Poincaré Duality and Circuit Duality

Now, let us introduce dual circuits. Consider a circuit on a planar graph. The planar graph is seen as a cellular paving \mathcal{K} for a two-dimensional plane (or a sphere surface). Because there is no nontrivial loop on a plane or sphere, we have the following equation:

$$\text{im}(\partial : C_2(\mathcal{K}) \rightarrow C_1(\mathcal{K})) = \ker(\partial : C_1(\mathcal{K}) \rightarrow C_0(\mathcal{K})). \quad (11)$$

Let $I \in Z_1(\mathcal{K})$ and $V \in B^1(\mathcal{K})$ be current and voltage distributions satisfying KCL and KVL, respectively. We set a reference resistance $R_{\text{ref}} (= 1/G_{\text{ref}})$ to exchange a current and voltage. Consider current $I^* := G_{\text{ref}}(\star^1)^{-1}(V)$ and voltage $V^* := R_{\text{ref}} \star_1(I)$ distributions for a circuit on \mathcal{K}^* , where $\star_1 : e_i \mapsto \check{e}^i$ and $(\star^1)^{-1} : e^i \mapsto \check{e}_i$ are defined with $\star^1 := (\star_1)^*$. Note that I^* and V^* are outer-oriented,

but we can obtain an inner-oriented component for a given orientation of the plane. By combining Equation (9) with Equation (11), KCL and KVL are shown to hold for I^* and V^* as explained below. Here, we check KVL for V^* . From Equation (11), a current distribution $I \in Z_1(\mathcal{K})$ can be written as $I = \partial F$ with “face” (or mesh) currents $F \in C_2(\mathcal{K})$. Then, we have $V^* = R_{\text{ref}} d(\star_2(F))$, which indicates $V^* \in B^1(\mathcal{K}^*)$. A similar discussion to KCL holds for I^* .

A current and voltage relation along a circuit element located at each edge $e_i \in \mathcal{E}$ is written by $h_i(I, V) = 0$ for $I \in Z_1(\mathcal{K})$, and $V \in B^1(\mathcal{K})$. As a dual relation, we define $h_i^*(I^*, V^*) := h_i(G_{\text{ref}}(\star_1)^{-1}(V^*), R_{\text{ref}} \star_1(I^*))$. If we assign a circuit element with $h_i^*(I^*, V^*) = 0$ for each edge e_i in \mathcal{K}^* , I^* and V^* give a solution of the circuit on \mathcal{K}^* . For example, consider a resistance with Ohm’s law $V = IR$ with scalar V, I , and R . Substituting $V \rightarrow I^*R_{\text{ref}}, I \rightarrow G_{\text{ref}}V^*$, we have $I^* = G^*V^*$ with $G^* = R/(R_{\text{ref}})^2$. Importantly, we obtain

$$RR^* = (R_{\text{ref}})^2 \tag{12}$$

for $R^* = 1/G^*$. The derived circuit on \mathcal{K}^* is called a *dual circuit*. The dual relation is summarized in Table 1.

Table 1. Dual relations in electrical circuits.

Circuit	Dual Circuit
Current distribution I	Voltage distribution $V^* = R_{\text{ref}} \star_1(I)$
Voltage distribution V	Current distribution $I^* = G_{\text{ref}}(\star_1)^{-1}(V)$
Face current F	Potential $\varphi^* = -R_{\text{ref}} \star_2(F)$
Potential φ	Face current $F^* = G_{\text{ref}}(\star_0)^{-1}(\varphi)$
Voltage source V_s	Current source $I_s^* = G_{\text{ref}}V_s$
Current source I_s	Voltage source $V_s^* = R_{\text{ref}}I_s$
Resistance R	Conductance $G^* = (G_{\text{ref}})^2R$
Conductance G	Resistance $R^* = (R_{\text{ref}})^2G$

For the previous example shown in Figure 17a, we construct a dual circuit as shown in Figure 17b. Here, we have $I_s^* = V_s/R_{\text{ref}}, R_i^* = (R_{\text{ref}})^2/R_i$, and take a specific orientation (\odot) of the plane to obtain an inner orientation of the current source. We can clearly see the duality between series and parallel connections in Figure 17. Therefore, the concept of dual circuits is considered as a generalization of series–parallel duality.

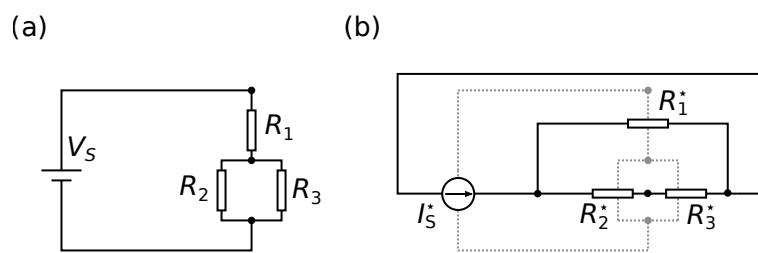


Figure 17. (a) example circuit and (b) its dual circuit.

■ Duality for Composite Resistances

Consider a one-port network N composed of resistors. A voltage source is attached to N as shown in Figure 18a. The network N is characterized by an equivalent resistance $R = V_s/I_s$, where V_s and I_s are the voltage and current along the source, respectively. Consider the dual counterpart as shown in Figure 18b. The dual network N^* is characterized by $R^* = V_s^*/I_s^*$ with the current I_s^* and voltage V_s^* along the source. From the corresponding duality, we have

$$RR^* = (R_{\text{ref}})^2, \tag{13}$$

where R_{ref} is the reference resistance.

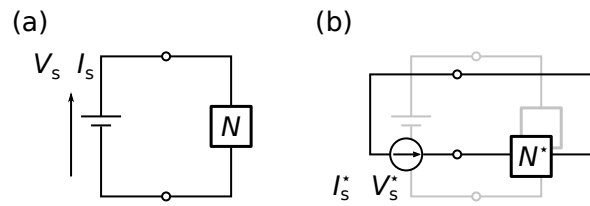


Figure 18. (a) one-port network with a voltage source and (b) its dual counterpart.

2.6. Self-Dual Circuit

If the *self-dual* relation $N = N^*$ holds for a one-port network N , the composite resistance satisfies $R = R^*$. In this case, we obtain $R = R^* = R_{\text{ref}}$ without solving circuit equations. As an example, we consider a bridge circuit shown in Figure 19a and its dual counterpart over R_{ref} is given in Figure 19b. The self-dual condition is written as $R_1 R_2 = (R_{\text{ref}})^2$. Under the self-dual condition, the circuit behaves as an effective resistor with R_{ref} .

Thus far, we only consider circuits with resistors, but the extension to alternating-current (AC) circuits is obvious. Under this extension, the real-number field (\mathbb{R}) is replaced with the complex one (\mathbb{C}). In AC circuits, resistances are replaced with complex impedances. Consider the example of an AC circuit shown in Figure 19c. This circuit is obtained from Figure 19a by replacing $R_1 \rightarrow Z_1 = j\omega L$, $R_2 \rightarrow Z_2 = 1/(j\omega C)$, where ω is an angular frequency. The self-dual condition is given by $R_{\text{ref}} = \sqrt{L/C}$. Under the self-duality, the circuit surprisingly behaves as a frequency-independent resistor with R_{ref} , although capacitors and inductors exhibit frequency-dependent response. This result can be interpreted to mean that the frequency dependency of capacitors and inductors negate each other when the whole system is self-dual. Therefore, self-dual circuits provide a powerful way to produce constant-resistance circuits [64].

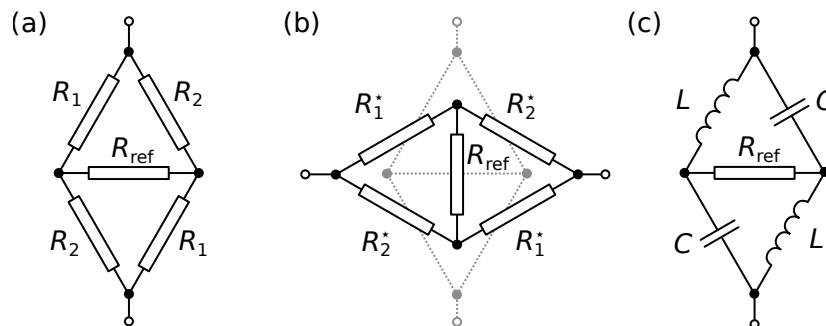


Figure 19. (a) bridge circuit and (b) its dual circuit; (c) alternating-current bridge circuit.

3. Zero Backscattering from Self-Duality

Signals can propagate in a uniform transmission line without backscattering. In this section, we associate self-duality with the zero-backscattering condition. Furthermore, we show that a large phase shift without backscattering in Huygens' metasurfaces can be understood by using a self-dual circuit model.

3.1. Self-Dual Transmission Lines

In this section, we consider signal propagation in a transmission line, which can be expressed by an LC ladder network [65]. In contrast to previous research on duality in transmission lines [66], we provide a circuit theoretical interpretation of the characteristic impedance of a transmission line in terms of self-dual response described in Section 2.

■ Telegraph Equations

A coaxial cable, which is composed of an inner conductor as a signal line and an outer conductor as a ground shield, forms capacitors between two conductors and inductors with a magnetic field around the inner conductor as shown in Figure 20a. With inductance \bar{L} and capacitance \bar{C} per unit length, the system is discretized as the LC ladder composed of $L_{i+\frac{1}{2}} = \bar{L}\Delta z$ and $C_i = \bar{C}\Delta z$ in a unit length Δz as shown in Figure 20b. In the i -th segment, Kirchhoff's voltage and current laws are, respectively, expressed as

$$L_{i-\frac{1}{2}} \frac{dI_{i-\frac{1}{2}}}{dt} = V_{i-1} - V_i, \tag{14}$$

$$C_i \frac{dV_i}{dt} = I_{i-\frac{1}{2}} - I_{i+\frac{1}{2}}. \tag{15}$$

In the continuum limit of $\Delta z \rightarrow 0$, the above equations become

$$\bar{L} \frac{\partial I}{\partial t} = -\frac{\partial V}{\partial z}, \tag{16}$$

$$\bar{C} \frac{\partial V}{\partial t} = -\frac{\partial I}{\partial z}, \tag{17}$$

which are well known as the telegraph equations. Generally, $\bar{L}(z)$ and $\bar{C}(z)$ can depend on z .

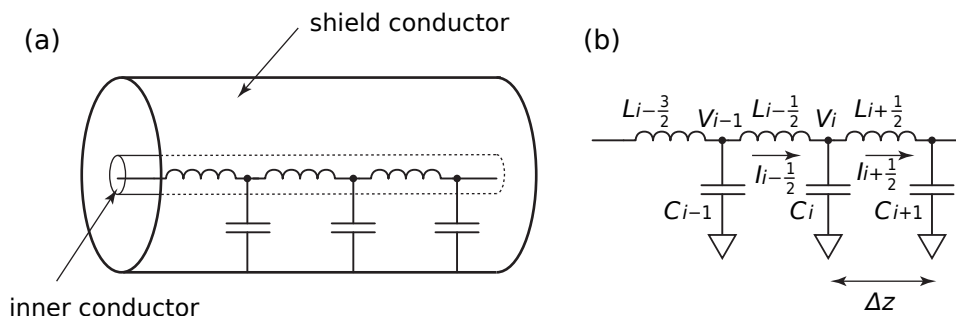


Figure 20. (a) coaxial cable and (b) its circuit model.

■ Zero Backscattering in Self-Dual Transmission Lines

Here, we see that the self-dual transmission line does not cause backscattering. If a transmission line has a constant impedance $Z = \sqrt{\bar{L}(z)/\bar{C}(z)}$ independent of z , then the transmission line becomes self-dual: the telegraph equations with a uniform Z are invariant under duality transformation $(V, I) \leftrightarrow (R_{\text{ref}}I, V/R_{\text{ref}})$ with $R_{\text{ref}} = Z$. In terms of the new variables $\eta_{\pm} = V \pm ZI$, the self-dual telegraph equations are written as

$$\frac{\partial \eta_{\pm}}{\partial z} \pm \frac{1}{v_0} \frac{\partial \eta_{\pm}}{\partial t} = 0, \tag{18}$$

where $v_0(z) = 1/\sqrt{\bar{L}\bar{C}}$. With arbitrary functions f_{\pm} , the general expression of the solution can be provided by $\eta_{\pm}(t, z) = f_{\pm}(t \mp \int^z dz'/v_0(z'))$, which corresponds to a propagating wave with velocity $\pm v_0(z)$ without backscattering. If $Z(z)$ depends on z , self-duality is broken and backscattering may be observed.

■ Circuit-Theoretical Derivation of Zero Backscattering

Next, we give a circuit-theoretical derivation of zero backscattering for a self-dual system. A transmission line composed of LC ladder circuits is shown in Figure 21a, where inductances

$L_{i+\frac{1}{2}}$ and capacitances C_i may depend on the position i . The dual circuit with respect to a global resistance R_{ref} is illustrated as shown in Figure 21b. The transformed circuit elements are given as

$$L_i^* = C_i(R_{\text{ref}})^2, \quad C_{i+\frac{1}{2}}^* = L_{i+\frac{1}{2}}/(R_{\text{ref}})^2. \tag{19}$$

In the limit of small L_i^* and $C_{i+\frac{1}{2}}^*$, each capacitance can be shifted to next position because the potential difference across each inductance is negligibly small. By repeating the shift of the capacitances $C_i \rightarrow C_{i+1}$ in the original circuit as shown in Figure 21c, we obtain the same circuit as Figure 21b ($L_i^* = L_{i+\frac{1}{2}}$ and $C_{i+\frac{1}{2}}^* = C_i$) under the following condition for any i :

$$R_{\text{ref}} = \sqrt{\frac{L_{i+\frac{1}{2}}}{C_i}}. \tag{20}$$

In other words, the LC ladder network with constant $L_{i+\frac{1}{2}}/C_i$ is self-dual for impedance inversion with respect to R_{ref} defined by Equation (20). In this way, the *global* parameter R_{ref} is linked with the *local* impedance $Z_i = \sqrt{L_{i+\frac{1}{2}}/C_i}$, which is defined by $L_{i+\frac{1}{2}}$ and C_i in each site.

Next, we consider excitation of the self-dual LC ladder by a voltage source V connected at the left-hand side as shown in Figure 21d. The dual circuit is illustrated in Figure 21e, where the current source is given by $I_s = V_s/R_{\text{ref}}$. By repeating the shift of the capacitances $C_i \rightarrow C_{i+1}$ as depicted in Figure 21f, Figure 21e can be identified with Figure 21f. As discussed in Section 2.6, the self-dual circuit is characterized by the effective resistance R_{ref} as shown in Figure 21g. Imagine that we connect a uniform transmission line (T1) with a characteristic impedance of R_{ref} to the half-infinite circuit (T2). When the signal propagates from T1 to T2, any backscattering does not appear due to the impedance matching.

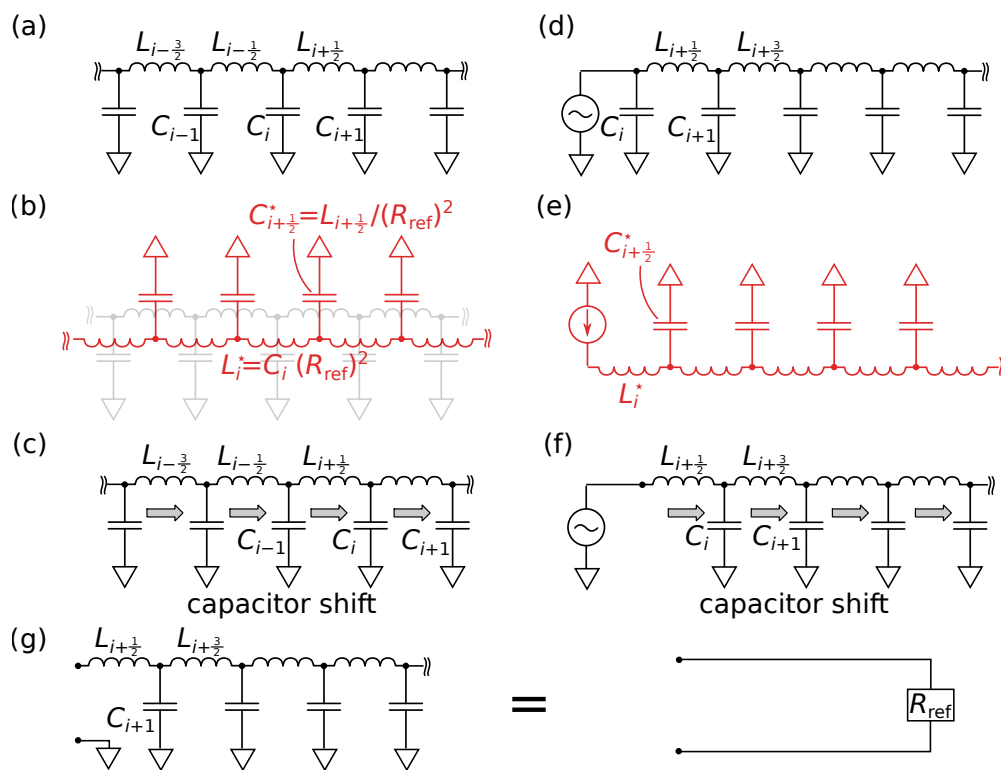


Figure 21. (a) LC ladder circuit and (b) its dual circuit; (c) capacitors in the circuit (a) are shifted; (d) LC ladder circuit excited by a voltage source and (e) its dual circuit; (f) capacitors in the circuit (d) are shifted; (g) input impedance of the LC ladder circuit.

■ Heaviside Condition

Self-duality can be realized in transmission lines with inductance $L_{i+\frac{1}{2}} = \bar{L}\Delta z$, capacitance $C_i = \bar{C}\Delta z$, conductance $G_i = \bar{G}\Delta z$, and resistance $R_{i+\frac{1}{2}} = \bar{R}\Delta z$ as shown in Figure 22. The self-dual condition is given by

$$\sqrt{\frac{\bar{L}}{\bar{C}}} = \sqrt{\frac{\bar{R}}{\bar{G}}}. \quad (21)$$

This self-dual condition is nothing but a no-distortion signal transmission condition derived by Heaviside [67]. Due to the self-duality, frequency-independent response is realized and backscattering vanishes, while a signal decays as it propagates.

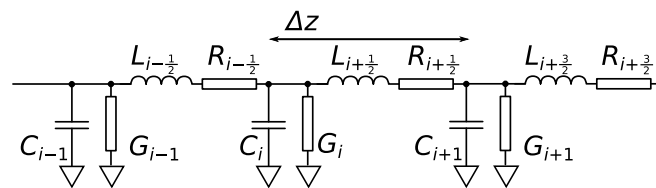


Figure 22. LC ladder with resistance and conductance.

3.2. Circuit Model for Huygens' Metasurface

Two-dimensional artificial structures called metasurfaces have been extensively investigated for controlling the amplitude and phase of transmitted and/or reflected electromagnetic waves [68]. The wavefront control of light can be realized by designing metasurfaces with spatial variations of phase responses [69–72]. The amplitude and phase responses of metasurfaces are generally interdependent. Nevertheless, it is possible to control the phase of the transmitted light with constant power transmission, which could be 100% in ideal conditions without losses, by carefully designing the resonant components of the metasurfaces. Metasurfaces for the arbitrary control of transmission properties, or amplitude and phase control, are called Huygens' metasurfaces, which have been introduced by Pfeiffer and Grbic [73]. In this subsection, we clarify the role of self-duality in Huygens' metasurfaces.

■ Transmission and Reflection for Huygens' Metasurfaces

It is assumed that monochromatic plane electromagnetic waves with a specific polarization are normally incident on an isotropic metasurface placed at $z = 0$ in a vacuum with a wave impedance of Z_0 . In this paper, the variable with a tilde represents the complex amplitude of a harmonically oscillating quantity $A = \tilde{A}e^{j\omega t} + \text{c.c.}$, where c.c. denotes the complex conjugate of the preceding term. The complex amplitudes of macroscopic electric and magnetic fields, which are averaged over the typical scale of metasurface elements, are represented by \tilde{E}_- and \tilde{H}_- (\tilde{E}_+ and \tilde{H}_+) for the input (output) side $z \leq 0$ ($z \geq 0$) in the proximity to the surface. Although electric and magnetic fields are represented by vectors, we here focus on scalar amplitudes for a specific polarization. Electromagnetic response of the metasurface is characterized by two parameters: electric sheet admittance Y_e and magnetic sheet impedance Z_m . The averaged electric fields $\tilde{E}_{\text{av}} = (\tilde{E}_- + \tilde{E}_+)/2$ induce surface currents $\tilde{K} = Y_e \tilde{E}_{\text{av}}$, which demand the boundary condition $\tilde{H}_- - \tilde{H}_+ = \tilde{K}$ on $z = 0$ [74]. In the same way, the magnetic counterpart can be considered, and the averaged magnetic fields $\tilde{H}_{\text{av}} = (\tilde{H}_- + \tilde{H}_+)/2$ produce surface magnetic currents $\tilde{K}_m = Z_m \tilde{H}_{\text{av}}$, which require the boundary condition $\tilde{E}_- - \tilde{E}_+ = \tilde{K}_m$. The boundary conditions are summarized as

$$\tilde{H}_- - \tilde{H}_+ = Y_e \frac{\tilde{E}_- + \tilde{E}_+}{2}, \quad (22)$$

$$\tilde{E}_- - \tilde{E}_+ = Z_m \frac{\tilde{H}_- + \tilde{H}_+}{2}. \quad (23)$$

For the incident wave propagating in the $+z$ direction with the electric field $\tilde{E}_{\text{in}} e^{-jkz}$ and the magnetic field $\tilde{H}_{\text{in}} e^{-jkz}$ ($= \tilde{E}_{\text{in}} e^{-jkz} / Z_0$), the total electric and magnetic fields (\tilde{E} , \tilde{H}) are represented as $(\tilde{E}_{\text{in}} e^{-jkz} + \rho \tilde{E}_{\text{in}} e^{jkz}, \tilde{H}_{\text{in}} e^{-jkz} - \rho \tilde{H}_{\text{in}} e^{jkz})$ in $z \leq 0$ and $(\tau \tilde{E}_{\text{in}} e^{-jkz}, \tau \tilde{H}_{\text{in}} e^{-jkz})$ in $z \geq 0$, where τ and ρ are the amplitude transmission and reflection coefficients. By substituting these fields at the metasurface ($z = 0$) into Equations (22) and (23), the amplitude transmission and reflection coefficients are obtained as

$$\begin{aligned}\tau &= \frac{(Z_2 - Z_1)Z_0}{(Z_0 + Z_1)(Z_0 + Z_2)}, \\ \rho &= \frac{Z_1 Z_2 - (Z_0)^2}{(Z_0 + Z_1)(Z_0 + Z_2)},\end{aligned}\quad (24)$$

where $Z_1 = Z_m/2$ and $Z_2 = 2/Y_e$. Hence, the reflection vanishes for $Z_1 Z_2 = (Z_0)^2$. In addition to the no-reflection condition, if Z_1 and Z_2 are purely imaginary impedances, which are expressed as $Z_1 = (Z_0)^2 / Z_2 = jbZ_0$ with a dimensionless number $b \in \mathbb{R}$, the transmission coefficient can be written as

$$\tau = \frac{1 - jb}{1 + jb}.\quad (25)$$

The incident waves are perfectly transmitted through the metasurface due to the fact that $|\tau|^2 = 1$ for any b , and the transmitted waves acquire a phase of $\theta = -2 \arctan b$. Such metasurfaces, which are typical examples of Huygens' metasurfaces, realize arbitrary phase shift θ without losses in an ideal case by tailoring the design of the metasurface structures. Both of the electric and magnetic responses are indispensable for the no-reflection condition.

■ Circuit Model for Huygens' Metasurfaces

The propagation of electromagnetic waves in a vacuum can be modeled as signal propagation in a transmission line with the wave impedance Z_0 , and the metasurface is represented by circuit elements inserted in the transmission line as shown in Figure 23a. In this model, the electric field \tilde{E} and magnetic field \tilde{H} are replaced with voltage \tilde{V} and current \tilde{I} , respectively; therefore, the circuit model of the metasurface should satisfy the following conditions:

$$\tilde{I}_- - \tilde{I}_+ = Y_e \frac{\tilde{V}_- + \tilde{V}_+}{2},\quad (26)$$

$$\tilde{V}_- - \tilde{V}_+ = Z_m \frac{\tilde{I}_- + \tilde{I}_+}{2}.\quad (27)$$

A circuit called a lattice circuit as shown in Figure 23b satisfies the above conditions [75]. The electric and magnetic responses are represented by impedances $Z_2 (= 2/Y_e)$ and $Z_1 (= Z_m/2)$, respectively. Equations (26) and (27) can be confirmed separately for Figure 23b, considering excitation by waves from both sides of the metasurface. For in-phase excitation $\tilde{V}_- = \tilde{V}_+$, all currents are sunk into the bridge circuit, and the currents become antiphase $\tilde{I}_- = -\tilde{I}_+$. There is no voltage across Z_1 , and the currents flow only in Z_2 . Hence, we obtain $\tilde{V}_- = Z_2 \tilde{I}_-$, which is identical to Equation (26) for $\tilde{V}_- = \tilde{V}_+$ and $\tilde{I}_- = -\tilde{I}_+$. In the opposite case, $\tilde{V}_- = -\tilde{V}_+$ and $\tilde{I}_- = \tilde{I}_+$, the currents flow only in Z_1 , and $\tilde{V}_- = Z_1 \tilde{I}_-$, so the equation that corresponds to Equation (27) can be derived.

■ Zero Backscattering Due to Self-Duality

For Figure 23a, $Z_{\text{in}} = \tilde{V}_- / \tilde{I}_-$ provides the input impedance for the metasurface, or lattice circuit, followed by the transmission line in $z > 0$. The uniform semi-infinite transmission line in $z > 0$ can be regarded as a resistor with an impedance of Z_0 as shown in Figure 21g. As a result, the total system viewed from the input side $z < 0$ is well described by a bridge circuit as shown in Figure 23c, and Z_{in} is identical to the impedance of the bridge circuit. As described in Section 2.6, the bridge circuit satisfying $Z_1 Z_2 = (Z_0)^2$ is self-dual for the inversion center Z_0 , and the input impedance Z_{in} is always Z_0 . The reflection vanishes under this condition, where the wave impedance Z_0 is impedance-matched to the load represented by the

bridge circuit. As a result, all energy is transmitted to the transmission line in $z > 0$. Thus, the no-reflection condition for Huygens' metasurfaces is interpreted in terms of self-duality.

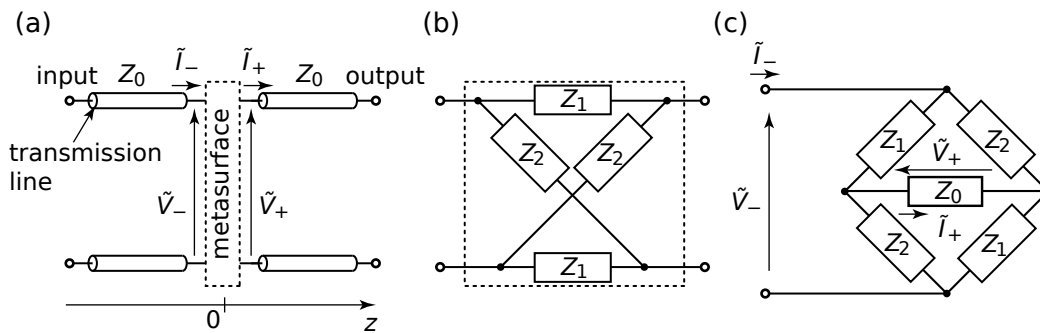


Figure 23. (a) circuit model for propagating electromagnetic waves incident on a metasurface; (b) circuit model of Huygens' metasurfaces with $Z_1 = Z_m/2$ and $Z_2 = 2/Y_e$; (c) lumped circuit model for the metasurface followed by a semi-infinite transmission line.

4. Keller–Dykhne Duality

Circuit duality can be extended for a continuous system. As with circuits, the effective response of a continuous system is associated with that of the dual one; thus, a self-dual response is automatically guaranteed. Such a constraint can induce critical behaviors of self-dual systems. Here, these topics are reviewed. Next, we introduce differential forms to clearly extract the structure of the duality in a continuous system. The correspondence between the dualities in continuous and discrete systems is formulated through discretization of continuous fields. In this section, we always use the right-hand vector product, in other words, \mathbf{A} , \mathbf{B} , and $\mathbf{A} \times \mathbf{B}$ obey the right-hand rule.

4.1. Two-Dimensional Resistive Sheets

Consider an electric field $\mathbf{E}(x, y)$ and current density $\mathbf{K}(x, y)$ on a two-dimensional resistive sheet located at $z = 0$ with a sheet conductance $G(x, y)$. Here, we assume that the fields inside the thin sheet are uniform along z and omit z -dependency for the fields. Thus, we treat the fields as two-dimensional vector fields independent of z . An example configuration is shown in Figure 24a. The physical dimensions of \mathbf{E} , \mathbf{K} , and G are V/m , A/m , and $1/\Omega$, respectively. From KVL and KCL, we obtain

$$\nabla \times \mathbf{E} = 0, \tag{28}$$

$$\nabla \cdot \mathbf{K} = 0. \tag{29}$$

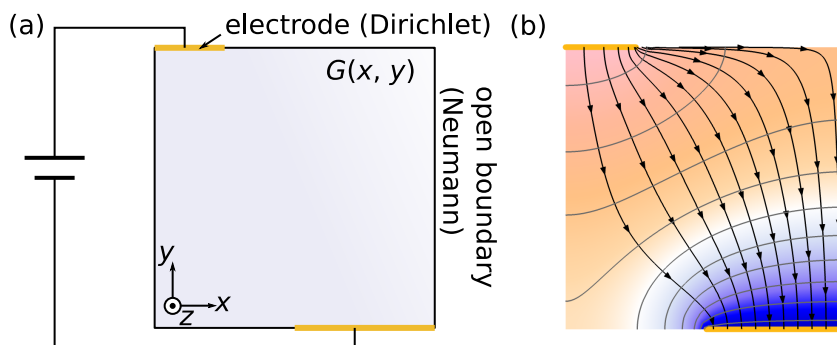


Figure 24. (a) two-dimensional resistive sheet with boundary conditions; (b) solution for a sheet with a constant sheet conductance $G(x, y) = G_{\text{ref}}$. Black lines represent the current flow. The potential is shown as a color map with isopotential gray contours.

Note that these equations can be directly obtained from Maxwell's equations; by omitting the time-derivative terms for steady states, we can obtain Equations (28) and (29) from Faraday's law and the law of charge conservation. Ohm's law is given by

$$\mathbf{K} = G\mathbf{E}, \quad (30)$$

where G is a conductance and generally a 2×2 matrix. For a metallic electrode, the boundary condition is written as

$$\mathbf{n} \times \mathbf{E} = 0, \quad (31)$$

where \mathbf{n} is the unit vector normal to the boundary. For an open boundary, the boundary condition is given by

$$\mathbf{n} \cdot \mathbf{K} = 0. \quad (32)$$

From Equation (28), the electric field is represented by

$$\mathbf{E} = -\nabla\varphi \quad (33)$$

with a potential $\varphi(x, y)$. Combining Equation (33) with Equations (29) and (30), we obtain

$$\nabla \cdot G\nabla\varphi = 0. \quad (34)$$

The boundary of the i -th electrode is specified by the Dirichlet boundary condition

$$\varphi = \varphi_i, \quad (35)$$

which is constant along the boundary. The open boundary is given by the Neumann boundary condition

$$\mathbf{n} \cdot G\nabla\varphi = 0. \quad (36)$$

For a simplified system with a constant scalar conductance, we have the Laplace equation

$$\nabla^2\varphi = 0 \quad (37)$$

from Equation (34). An example solution of the Laplace equation calculated by COMSOL Multiphysics[®] is shown in Figure 24b.

4.2. Duality in Laplace Equation

In this subsection, we discuss duality in Laplace equations [76]. The solution of the Laplace equation is called a *harmonic function*. A harmonic function can be considered as a part of a holomorphic function. To see this fact, consider a holomorphic function $w(z) = u(z) + jv(z)$ with $z = x + jy$, $u(z) = \text{Re}[w(z)]$, and $v(z) = \text{Im}[w(z)]$. The holomorphism leads to the Cauchy–Riemann equations:

$$\frac{\partial u}{\partial x} = \frac{\partial v}{\partial y} \quad (38)$$

$$\frac{\partial u}{\partial y} = -\frac{\partial v}{\partial x}. \quad (39)$$

These equations can be expressed as

$$\begin{bmatrix} \frac{\partial v}{\partial x} \\ \frac{\partial v}{\partial y} \end{bmatrix} = J \begin{bmatrix} \frac{\partial u}{\partial x} \\ \frac{\partial u}{\partial y} \end{bmatrix} \quad (40)$$

with $J = \begin{bmatrix} 0 & -1 \\ 1 & 0 \end{bmatrix}$, which induces counterclockwise 90° rotation. As we differentiate Equations (38) and (39) along x and y , respectively, and combine the results, we obtain

$$\nabla^2 u = 0, \tag{41}$$

which states that u is harmonic. Similarly, v is also harmonic. Here, v is called a *harmonic conjugate* of u .

If u is given, how can we obtain its harmonic conjugate v ? Focusing on $v(x, y) = v(x_0, y_0) + \int_{\text{path}:(x_0, y_0) \rightarrow (x, y)} (\nabla v) \cdot d\mathbf{r}$ with Equation (40), we have

$$v(x, y) = v(x_0, y_0) + \int_{\text{path}:(x_0, y_0) \rightarrow (x, y)} (J\nabla u) \cdot d\mathbf{r}, \tag{42}$$

where $\mathbf{r} = [x \ y]^T$ and (x_0, y_0) is a fixed point. We have assumed that the considered region is simply connected to define Equation (42). When we consider a small displacement $\Delta\mathbf{r}$ along a line $v(x, y) = \text{const.}$, we have $(J\nabla u) \cdot \Delta\mathbf{r} = 0$, which leads to $\nabla u \parallel \Delta\mathbf{r}$. Therefore, u and v constitute an orthogonal coordinate around the point $\nabla u \neq 0$, as shown in Figure 25a. In this subsection, the operation of taking the harmonic conjugate is treated as a duality transformation.

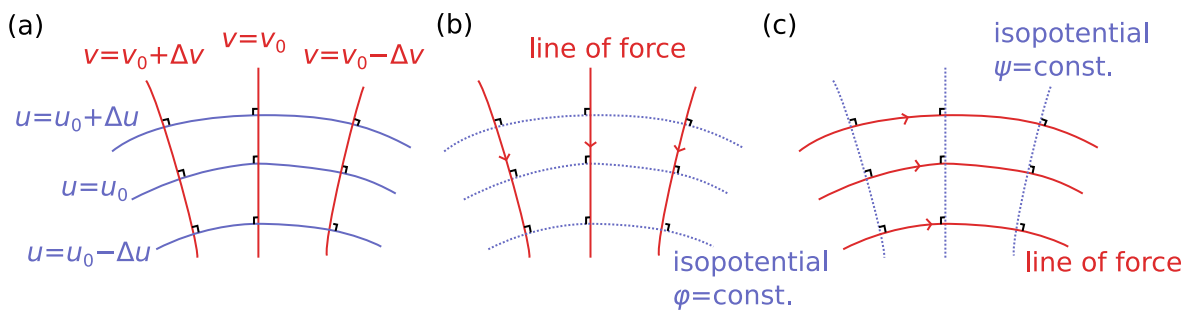


Figure 25. (a) holomorphic function $w(z) = u(z) + jv(z)$ defines an orthogonal coordinate around a point with $dw/dz \neq 0$; (b) harmonic potential ϕ and the lines of force $-\nabla\phi$; (c) harmonic conjugate ψ for ϕ and the lines of force $-\nabla\psi$.

The above result induces duality for the potential problem of the Laplace equation. Let ψ be the harmonic conjugate of a harmonic potential ϕ . The relation between ϕ and ψ is depicted in Figure 25b,c. Now, we come back to resistive sheet problems. The current stream lines and isopotential contours are replaced with each other under the harmonic conjugate as shown in the simplest example of Figure 26. Furthermore, we can see that the harmonic conjugate interchanges the Dirichlet and the Neumann boundary conditions because of the 90° rotation.

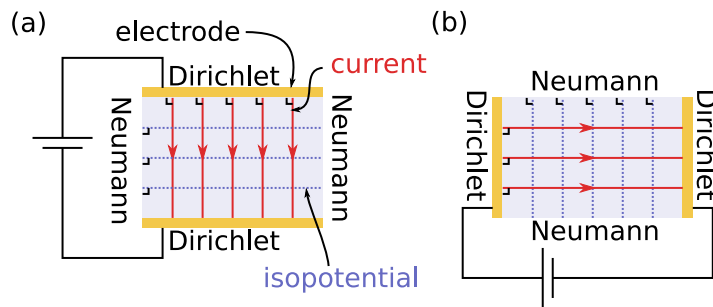


Figure 26. Current and potential distributions for (a) original and (b) its dual resistive sheets with a uniform conductance.

4.3. Generalized Duality

Harmonic duality can be extended to a two-dimensional resistive sheet with a spatially inhomogeneous sheet conductance $G(x, y)$. Keller proved the duality for a system composed of two different conductances [6], and Dykhne generalized it to a system with an arbitrary scalar function $G(x, y)$ [7]. The extended duality is often called *Keller–Dykhne duality*. Furthermore, Mendelson generalized the duality for a tensor $G(x, y)$ [8].

Here, we review the derivation of the duality. As with circuit duality, we set a reference resistance $R_{\text{ref}} (= 1/G_{\text{ref}})$. Referring to a 90° rotation in Equation (40), we introduce the following dual fields on $z = 0$:

$$\mathbf{E}^* = R_{\text{ref}} \mathbf{J} \mathbf{K} = R_{\text{ref}} \mathbf{e}_z \times \mathbf{K}, \quad (43)$$

$$\mathbf{K}^* = G_{\text{ref}} \mathbf{J} \mathbf{E} = G_{\text{ref}} \mathbf{e}_z \times \mathbf{E}, \quad (44)$$

with the unit vector \mathbf{e}_z along the z direction. The 90° rotation interchanges divergence and rotation of a two-dimensional vector field $\mathbf{v}(x, y)$ as

$$\nabla \times (\mathbf{e}_z \times \mathbf{v}) = \mathbf{e}_z \nabla \cdot \mathbf{v}, \quad (45)$$

$$\nabla \cdot (\mathbf{e}_z \times \mathbf{v}) = -\mathbf{e}_z \cdot (\nabla \times \mathbf{v}), \quad (46)$$

where we used $\nabla \times (\mathbf{A} \times \mathbf{B}) = \mathbf{A}(\nabla \cdot \mathbf{B}) - \mathbf{B}(\nabla \cdot \mathbf{A}) + (\mathbf{B} \cdot \nabla) \mathbf{A} - (\mathbf{A} \cdot \nabla) \mathbf{B}$ and $\nabla \cdot (\mathbf{A} \times \mathbf{B}) = \mathbf{B} \cdot (\nabla \times \mathbf{A}) - \mathbf{A} \cdot (\nabla \times \mathbf{B})$. Thus, KVL and KCL for \mathbf{E}^* and \mathbf{K}^* automatically follow: $\nabla \times \mathbf{E}^* = 0$ and $\nabla \cdot \mathbf{K}^* = 0$. In addition, Ohm's law in Equation (30) is converted to

$$\mathbf{K}^* = G^* \mathbf{E}^* \quad (47)$$

with

$$G^* = (G_{\text{ref}})^2 \mathbf{J} G^{-1} \mathbf{J}^{-1}. \quad (48)$$

For $R = G^{-1}$ and $R^* = (G^*)^{-1}$, we obtain

$$R^* \mathbf{J} R \mathbf{J}^{-1} = (R_{\text{ref}})^2. \quad (49)$$

Therefore, \mathbf{E}^* and \mathbf{K}^* give a solution for the sheet with G^* under interchanging the Dirichlet and Neumann boundary conditions. Note that G can be a tensor. For a scalar G , we simply obtain $G^* G = (G_{\text{ref}})^2$.

4.4. Effective Response and Duality

Duality can relate the effective response of an original sheet with its dual counterpart. To see this statement, consider a resistive sheet with two terminals as shown in Figure 27a. Between electrodes, we have the voltage $V = -\int_{c_1} \mathbf{E} \cdot d\mathbf{r}$ and current flow $I = \int_{c_2} \mathbf{K} \cdot \mathbf{n}_2 dr$. The effective conductance between the terminals is defined as $G_{\text{eff}} = I/V$. The dual system is also shown in Figure 27b, and the voltage and current are represented by $V^* = -\int_{c_2} \mathbf{E}^* \cdot d\mathbf{r}$ and $I^* = \int_{c_1} \mathbf{K}^* \cdot \mathbf{n}_1 dr$, respectively. Using $\mathbf{A} \cdot (\mathbf{B} \times \mathbf{C}) = \mathbf{B} \cdot (\mathbf{C} \times \mathbf{A}) = \mathbf{C} \cdot (\mathbf{A} \times \mathbf{B})$, we obtain

$$V^* = R_{\text{ref}} I, \quad (50)$$

$$I^* = G_{\text{ref}} V. \quad (51)$$

Therefore, the effective conductance G_{eff}^* for the dual system is given by

$$G_{\text{eff}}^* G_{\text{eff}} = (G_{\text{ref}})^2. \quad (52)$$

If the system is self-dual and passive, which means that there is no active element with a negative resistance, then $G_{\text{eff}} = G_{\text{eff}}^* = G_{\text{ref}}$ automatically follow. Thus, self-duality determines the effective response regardless of the structural geometry.

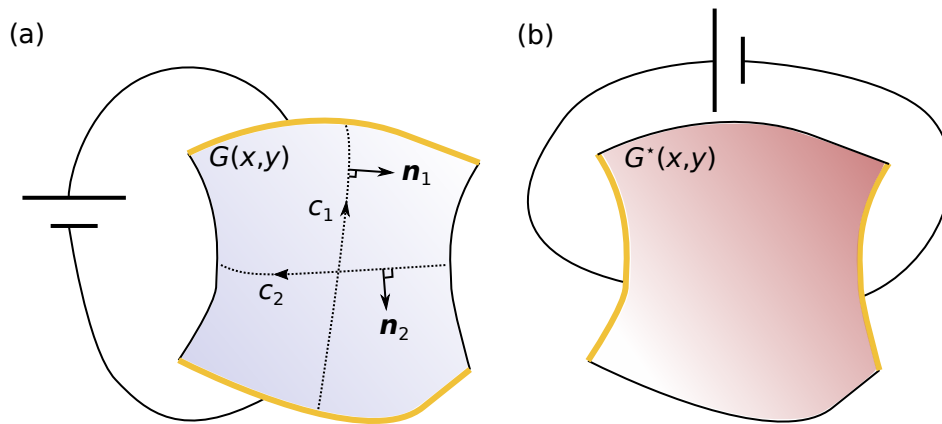


Figure 27. (a) resistive sheet with a sheet conductance $G(x, y)$ and two terminals; (b) corresponding counterpart with $G^* = (G_{\text{ref}})^2 J G^{-1} J^{-1}$. Unit normal vectors are denoted by n_1 and n_2 for curves c_1 and c_2 , respectively.

4.5. Self-Duality and Singularity

The self-dual effective response can sometimes predict a critical behavior of the system. To see how critical behavior appears in self-dual systems, we consider an ideal checkerboard with different admittances Y_1 and Y_2 , as shown in Figure 28a. Here, the AC response with an angular frequency ω is discussed for the checkerboard. For a capacitive admittance $Y_1 = j\omega C$ and an inductive admittance $Y_2 = (j\omega L)^{-1}$, the checkerboard is self-dual with respect to a reference conductance $G_{\text{ref}} = \sqrt{Y_1 Y_2} = \sqrt{C/L}$. Then, we obtain a real effective admittance $Y_{\text{eff}} = G_{\text{ref}}$ due to the self-duality. The positive real admittance indicates that the system is lossy. However, the system is lossless because the effective admittance composed only of capacitors and inductors must be purely imaginary. Therefore, we do not have a physical solution for such a checkerboard composed of capacitors and inductors. Thus, the lossless ideal checkerboard is *singular*.

The above observation can be also interpreted from a branch cut for the self-dual admittance $Y_{\text{eff}}(Y_1, Y_2) = \sqrt{Y_1 Y_2}$ [77]. We fix Y_2 at a point of the negative imaginary axis and gradually displace Y_1 from Y_2 as shown in Figure 28b. When we consider $Y_{\text{eff}}(Y_1) = \sqrt{Y_1 Y_2}$ as a function of Y_1 , $Y_{\text{eff}}(Y_1)$ must have a branch cut in the complex plane. The previous discussion clearly shows that the branch cut is located along the positive imaginary axis. This result indicates that two approaches from $\text{Re}(Y_1) > 0$ and $\text{Re}(Y_1) < 0$ regions to a point at the singular branch lead to different values of Y_{eff} . The effective admittance on the branch is critically sensitive to loss or gain of the system.

The above result can be generalized for arbitrary Y_2 . Using linearity

$$Y_{\text{eff}}(sY_1, sY_2) = sY_{\text{eff}}(Y_1, Y_2) \quad (53)$$

for a scalar s , we can write Y_{eff} as $Y_{\text{eff}} = Y_2 R_{\text{ref}} Y_{\text{eff}}(\eta G_{\text{ref}}, G_{\text{ref}})$ with $\eta = Y_1/Y_2$. Therefore, all system characteristics are derived from $y_{\text{eff}}(\eta) := R_{\text{ref}} Y_{\text{eff}}(\eta G_{\text{ref}}, G_{\text{ref}})$ satisfying $y_{\text{eff}}(\eta) = \eta y_{\text{eff}}(\eta^{-1})$ due to the self-duality $Y_{\text{eff}}(Y_1, Y_2) = Y_{\text{eff}}(Y_2, Y_1)$. Because singular Y_1 is represented by $Y_1 = sY_2 (s < 0)$ in the previous discussion, self-dual $y_{\text{eff}}(\eta)$ has a branch cut along the negative real axis of η .

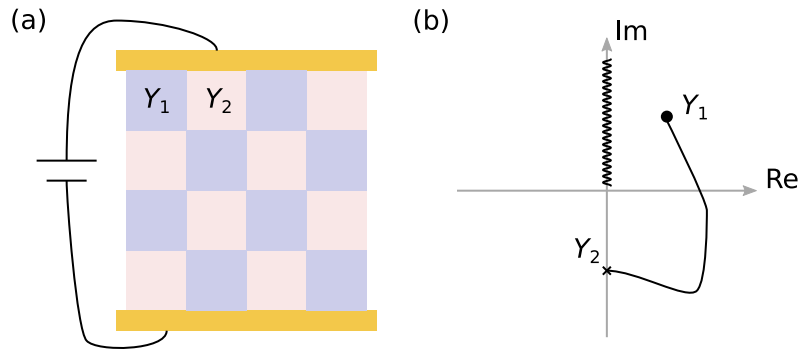


Figure 28. (a) ideal checkerboard sheet with sheet admittances Y_1 and Y_2 ; (b) domain of definition for the effective admittance $Y_{\text{eff}}(Y_1) = \sqrt{Y_1 Y_2}$. The branch cut along the positive imaginary axis is indicated by a wavy line.

4.6. Differential-Form Approach for Duality

Although Keller–Dykhne duality was formulated through vector analysis, the essence of the duality can be vividly extracted by differential forms. Furthermore, differential forms are suitable to discretize continuous fields to circuit systems. Discretizing differential forms, we bridge between Keller–Dykhne duality and circuit duality.

Here, let us introduce differential forms and the exterior derivative in plain terms. To this end, we only focus on Cartesian coordinates. For more technical details of differential forms, see [59,78].

■ Covector and 1-Form

First, consider an electric field at a point (x_0, y_0) . The Cartesian basis is denoted by $\{e_x, e_y\}$. A displacement $\Delta r = \Delta x e_x + \Delta y e_y$ and the electric potential difference $\Delta\varphi$ are related through

$$-\Delta\varphi = E_x(x_0, y_0)\Delta x + E_y(x_0, y_0)\Delta y. \tag{54}$$

It is possible to consider an electric field E as a linear function as $E : \Delta r \mapsto -\Delta\varphi$. Physically, we may understand the electric field as an apparatus that measures the (minus) electric potential difference for a displacement Δr . Such a linear map from a vector to a scalar is called a *covector*. Introducing a dual basis $\{dx, dy\}$ with respect to the Cartesian basis $\{e_x, e_y\}$, we can write the covector as

$$E(x_0, y_0) = E_x(x_0, y_0)dx + E_y(x_0, y_0)dy. \tag{55}$$

The action of the *interior product* between $E(x_0, y_0)$ and a displacement vector Δr is written as

$$\Delta r \lrcorner E(x_0, y_0) = E_x(x_0, y_0)\Delta x + E_y(x_0, y_0)\Delta y. \tag{56}$$

From the definition, we have $e_x \lrcorner dx = 1$, $e_y \lrcorner dx = 0$, $e_x \lrcorner dy = 0$, and $e_y \lrcorner dy = 1$. A covector α should be depicted as a set of parallel lines with an outer orientation as shown in Figure 29a. As the covector becomes stronger, the lines become denser. The interior product $v \lrcorner \alpha$ gives the signed number of lines that the vector v pierces. Note that we consider a limit operation in the strict sense as follows: we set a small resolution value ϵ and define a set of lines $\{L_m | m \in \mathbb{Z}\}$ with $L_m = \{r | r \lrcorner \alpha = m\epsilon\}$. The number of the lines of $\{L_m\}$ pierced by v is denoted as $N(\epsilon)$. Then, we obtain $v \lrcorner \alpha = \lim_{\epsilon \rightarrow 0} \epsilon N(\epsilon)$.

The electric field is given by a covector field

$$E(x, y) = E_x(x, y)dx + E_y(x, y)dy, \tag{57}$$

which smoothly depends on (x, y) . Covector fields are generally called *1-forms*. An example of a 1-form is shown in Figure 29b. For a general 1-form α , $v \lrcorner \alpha$ is evaluated at the tangent space to which

v belongs: $v \lrcorner \alpha = v \lrcorner \alpha(x_0, y_0)$ for v whose starting point is (x_0, y_0) . The 1-form α can be integrated along a curve c as

$$\int_c \alpha := \lim_{N \rightarrow \infty} \sum_{i=0}^{N-1} \Delta r_i \lrcorner \alpha, \tag{58}$$

where curve $c(t) : [0, 1] \rightarrow \mathbb{E}_2$ is discretized as $\Delta r_i = c(t_{i+1}) - c(t_i)$ with $t_i = i/N$ (\mathbb{E}_2 : two-dimensional Euclidean space). Note that Δr_i is considered to be in the tangent space of $c(t_i)$. This definition can be linearly extended for any 1-chain c , and a 1-form is considered as a 1-cochain. By integrating, we can express a voltage difference as $V = - \int_c E$.

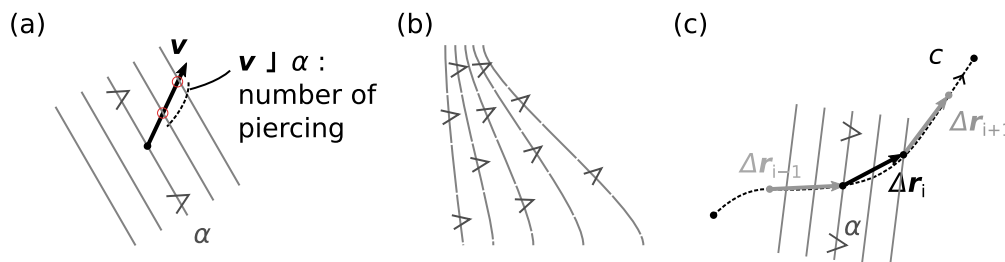


Figure 29. (a) illustration of a covector α . The signed number of lines that a vector v pierces is given by $v \lrcorner \alpha$. The positive direction of α is depicted by carets; (b) covector field (1-form); (c) discretized curve c with displaced vectors Δr_i to define the integral of a 1-form α along c .

■ Tensors and Products

Similar to a covector, a (covariant) tensor maps p input vectors to a scalar output: $T(v_1, v_2, \dots, v_p)$, which has linearity in each slot. The interior product of a vector v and a tensor T can be defined as $v \lrcorner T = T(v, \square, \dots)$, which indicates that the first slot is filled with v and the other slots are left waiting for inputs (\square).

To obtain a higher-order tensor, other products are introduced. First, the tensor product of two covectors α and β is defined as follows: $\alpha \otimes \beta(u, v) = \alpha(u)\beta(v)$ for u, v in a vector space U . For 1-forms, the tensor product operates on each tangent space.

Second, the wedge product for two 1-forms α and β is defined as an antisymmetrized tensor

$$\alpha \wedge \beta = \frac{1}{2}(\alpha \otimes \beta - \beta \otimes \alpha). \tag{59}$$

The wedge product of two 1-forms satisfies

$$\alpha \wedge \beta = -\beta \wedge \alpha, \tag{60}$$

$$\alpha \wedge \alpha = 0. \tag{61}$$

As $dx \wedge dx = dy \wedge dy = 0$, only $dx \wedge dy$ plays an important role. For $u = u^x e_x + u^y e_y$ and $v = v^x e_x + v^y e_y$, we have

$$dx \wedge dy(u, v) = \frac{1}{2} \det \begin{bmatrix} u^x & v^x \\ u^y & v^y \end{bmatrix}. \tag{62}$$

Due to the antisymmetry $dx \wedge dy(u, v) = -dx \wedge dy(v, u)$, $dx \wedge dy$ measures a signed area of a triangle spanned by u and v . In Figure 30a, we illustrate $dx \wedge dy$ as directed circles and $dx \wedge dy(u, v)$ counts the number of circles inside the triangle spanned by u and v . If the direction from u to v is the same (opposite) as the direction of the circles, the circles are counted as positive (negative) numbers.

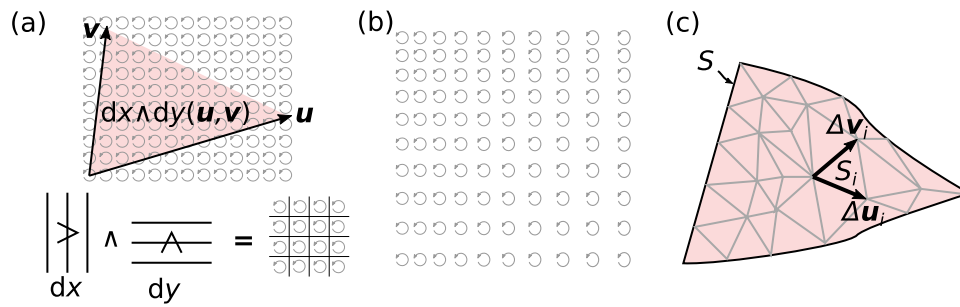


Figure 30. (a) $dx \wedge dy$ as directed circles; (b) example of a 2-form; (c) discretization for integration.

■ 2-Forms and Integration

We can also consider a field $\omega = f(x, y)dx \wedge dy$ with a scalar function $f(x, y)$, where ω is called a 2-form. An example of a 2-form is shown in Figure 30b, where the dense circle area has a stronger field than the sparse area. For integration, we discretize a directed 2-cell S as $S = \cup_i S_i$ with disjoint small triangles S_i (Figure 30c). A 2-form can be integrated on S as

$$\int_S \omega = \lim \sum_i f(x_i, y_i) \omega(\Delta u_i, \Delta v_i), \tag{63}$$

where Δu_i and Δv_i span a triangle S_i with the same direction of S and $(x_i, y_i) \in S_i$. The limit is taken for finer meshes. Generally, S can be an arbitrary 2-chain. Then, a 2-form can be considered as a 2-cochain. Note that integration of a general tensor T without antisymmetry cannot be defined and the antisymmetry is essential for integration. To define the integral, the integration over subdivided triangles should be the same as that of the original triangle. At least, $T(u, v) = T(u, \frac{u+v}{2}) + T(\frac{u+v}{2}, v)$ is required for arbitrary u and v . Considering $u = v$, we obtain $T(u, u) = 0$ for arbitrary u . Then, the antisymmetry $T(u, v) = -T(v, u)$ must hold due to $T(u + v, u + v) = 0$.

■ Exterior Derivative

The exterior derivative for a scalar function $f(x, y)$ is defined as

$$df = \frac{\partial f}{\partial x} dx + \frac{\partial f}{\partial y} dy, \tag{64}$$

which corresponds to the gradient of the function f . For a 1-form $\alpha = \alpha_x dx + \alpha_y dy$, we define the exterior derivative as

$$d\alpha = (d\alpha_x) \wedge dx + (d\alpha_y) \wedge dy. \tag{65}$$

By direct calculation,

$$d\alpha = \left(\frac{\partial \alpha_y}{\partial x} - \frac{\partial \alpha_x}{\partial y} \right) dx \wedge dy,$$

this corresponds to a rotation. By using the exterior derivative, KVL is represented as $dE = 0$.

■ Stokes' Theorem

How may one relate an exterior derivative to the boundary of a chain? Green's theorem

$$\oint_{\partial S} (f dx + g dy) = \iint_S \left(\frac{\partial g}{\partial x} - \frac{\partial f}{\partial y} \right) dx dy \tag{66}$$

can be rewritten as the following equation for a 2-chain S with a 1-form α :

$$\int_S d\alpha = \int_{\partial S} \alpha. \tag{67}$$

Equation (67) generally holds for higher-dimensional spaces, and it is known as Stokes' theorem. Stokes' theorem relates the boundary operator ∂ with the exterior derivative d .

■ Twisted 1-Form

Next, we consider a representation of current density. As discussed in Section 2.3, current flow should be calculated for an outer-oriented 1-chain, so the current density is an outer-oriented 1-cochain. The outer-oriented 1-chain \check{c} was represented as $\check{c} = \{\check{c}_o | o = \circlearrowleft, \circlearrowright\}$ by using the inner-oriented 1-chain \check{c}_o depending on a plane orientation o . Thus, current density K should be represented as $K = \{K_o | o = \circlearrowleft, \circlearrowright\}$ with the two 1-forms satisfying

$$K_{-o} = -K_o, \tag{68}$$

where $-o$ represents the opposite orientation of o . The set of two 1-forms satisfying Equation (68) is called a *twisted* 1-form. On the other hand, ordinary forms are called *untwisted*. A twisted 1-form $\check{\alpha}$ at a point P is an outer-oriented covector $\check{\alpha}_P$, which is depicted as the inner-oriented lines in Figure 31a. To stress the twist, we put the check symbol ($\check{\cdot}$) for twisted objects, but sometimes omit the mark to reduce the notation complexity. In Figure 31b, the twisted 1-form K is depicted by (local) stream lines. We can count the total current flow across a curve by the integration. The integration of K along an outer-oriented 1-chain \check{c} is defined as

$$\int_{\check{c}} K := \int_{\check{c}_o} K_o. \tag{69}$$

The exterior derivative of K is also defined as

$$(dK)_o = dK_o. \tag{70}$$

KCL states that

$$\int_{\partial\check{S}} K = \int_{\check{S}} dK = 0 \tag{71}$$

for any outer-oriented 2-cell \check{S} . Considering small \check{S} , we obtain $dK = 0$ as KCL.

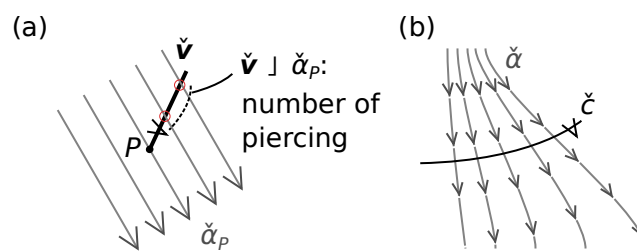


Figure 31. (a) interior product between an outer-oriented vector \check{v} and an outer-oriented covector $\check{\alpha}_P$ at a point P ; (b) integration of a twisted 1-form $\check{\alpha}$ along an outer-oriented 1-chain \check{c} .

■ Metric Tensor

To express Ohm's law, we will define the Hodge star operation. To define the Hodge star operation, we need to introduce a metric tensor. In the two-dimensional Euclidean space \mathbb{E}_2 , we can define the inner product of vectors $\mathbf{u} = u^x \mathbf{e}_x + u^y \mathbf{e}_y$ and $\mathbf{v} = v^x \mathbf{e}_x + v^y \mathbf{e}_y$ as

$$g(\mathbf{u}, \mathbf{v}) = \mathbf{u} \cdot \mathbf{v} \tag{72}$$

with $\mathbf{u} \cdot \mathbf{v} = u^x v^x + u^y v^y$. Here, g is called the *metric tensor*. We can define a covector $g^b(\mathbf{u})$ for a vector \mathbf{u} satisfying

$$g^b(\mathbf{u}) = g(\mathbf{u}, \square). \tag{73}$$

Therefore, $v \lrcorner g^b(u) = g(u, v)$ holds. The operation of g^b on e_x and e_y is graphically shown in Figure 32. The inverse map of g^b is written as $g^\sharp = (g^b)^{-1}$.

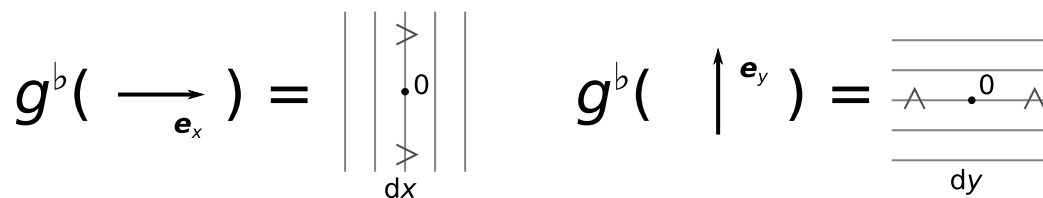


Figure 32. Conversion between a vector and a covector.

■ Area Form as a Twisted 2-Form

With respect to the metric of \mathbb{E}_2 , $\{e_x, e_y\}$ is an orthogonal basis: $g(e_i, e_j) = \delta_{ij}$ (δ_{ij} : Kronecker delta). Using the orthogonal coordinate, we can define a twisted 2-form “Area” as

$$\text{Area}_\circ = dx \wedge dy, \tag{74}$$

$$\text{Area}_\circ = -dx \wedge dy. \tag{75}$$

The area form measures the *unsigned* area of an outer-oriented 2-chain.

■ Hodge Star

Now, we define the Hodge star operation for a 1-form α as

$$(\star\alpha)_o = g^\sharp(\alpha) \lrcorner \text{Area}_o \tag{76}$$

with respect to an orientation o of the plane. The star operator \star maps a 1-form to a twisted 1-form. Naturally, we can define a Hodge star operation for a twisted 1-form $\check{\alpha}$ as:

$$\star \check{\alpha} = g^\sharp(\check{\alpha}_o) \lrcorner \text{Area}_o. \tag{77}$$

Then, the Hodge operator maps a twisted 1-form to an untwisted 1-form. The multiple operations of \star are shown in Figure 33. In this figure, we can see

$$\star \star = -\text{Id}, \tag{78}$$

where Id is the identity operator. Therefore, \star defines the complex structure in the two-dimensional plane. By using the Hodge star, we can represent Ohm’s law with a scalar sheet conductance G as $K = G \star E$. Note that the Hodge operator can be defined for other p -forms, but the sign of $\star\star$ generally depends on the order p , the dimension of the space, and the metric signature, rather than Equation (78) [59].

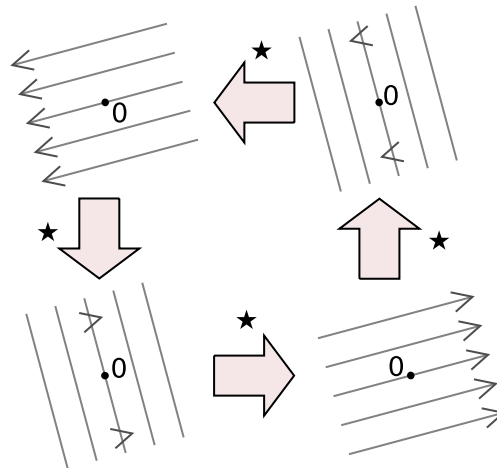


Figure 33. Complex structure of Hodge operations for untwisted and twisted 1-forms.

4.7. Summary of Basic Equations in Differential-Form Approach

Now, we summarize the basic equations with differential forms for a two-dimensional resistive sheet with a nonuniform scalar conductance. The electric field is represented by a 1-form E , while the current density field is given by a twisted 1-form K . KVL and KCL are formulated as

$$dE = 0, \tag{79}$$

$$dK = 0, \tag{80}$$

respectively. The scalar Ohm’s law is rewritten as

$$K = G \star E \tag{81}$$

with a scalar sheet conductance $G(= 1/R)$. These equations are schematically shown in Figure 34. Although we only focused on Cartesian coordinates, Equations (79)–(81) are coordinate free. Therefore, we can use an arbitrary coordinate for analysis. Another feature of the differential-form formalism is the exclusion of the metric in Equations (79) and (80). The metric appears through the Hodge star in Equation (81). Thus, Equations (79) and (80) are metric-free equations and easy to be discretized while keeping the geometrical structure, as we see later.

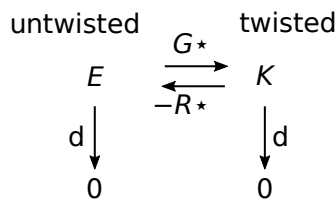


Figure 34. Structure of basic equations in a two-dimensional resistive sheet.

4.8. Keller–Dykhne Duality with Differential Forms

Now, we formulate Keller–Dykhne duality with differential forms. Electric and current fields are represented by untwisted and twisted 1-forms, respectively. To exchange these fields with two different kinds of orientations, we need to fix an orientation ω of the plane. Here, we define a twisted scalar $\Omega^\omega = \{(\Omega^\omega)_o | o = \circlearrowleft, \circlearrowright\}$ satisfying $(\Omega^\omega)_\omega = +1$ and $(\Omega^\omega)_{-\omega} = -1$. The pseudoscalar Ω^ω is

regarded as the plane orientation ω . For a twisted form $\check{\omega}$, Ω^ω extracts the component $\Omega^\omega \check{\omega} = \check{\omega}_\omega$. Now, we consider the replacement as

$$E^* = R_{\text{ref}} \Omega^\omega K, \quad (82)$$

$$K^* = -G_{\text{ref}} \Omega^\omega E \quad (83)$$

with respect to a reference resistance $R_{\text{ref}} (= 1/G_{\text{ref}})$. Clearly, these fields satisfy

$$dE^* = 0, \quad (84)$$

$$dK^* = 0. \quad (85)$$

From Equation (81) with Equations (82) and (83), we obtain

$$K^* = G^* \star E^*, \quad (86)$$

where we use Equation (78) and $G^* = (G_{\text{ref}})^2/G$ for a scalar G .

4.9. Discretization

Discretizing a two-dimensional sheet, we can obtain circuit duality again. In this subsection, we rigorously confirm this statement.

■ Discretization

For a sheet region U , we consider a cellular paving \mathcal{K} with nodes \mathcal{N} , edges \mathcal{E} , and faces \mathcal{F} . We write the relations among nodes, edges, and faces as

$$\partial e_i = \sum_{j=1}^{|\mathcal{N}|} n_j \Delta^j_i \quad (i = 1, 2, \dots, |\mathcal{E}|), \quad (87)$$

$$\partial f_i = \sum_{j=1}^{|\mathcal{E}|} e_j \Pi^j_i \quad (i = 1, 2, \dots, |\mathcal{F}|) \quad (88)$$

for $e_i \in \mathcal{E}$ and $f_i \in \mathcal{F}$. The totality of p -forms on U is denoted by $C^p(U)$. We can define $\phi^p : C^p(U) \rightarrow C^p(\mathcal{K})$ as

$$[\phi^p(\omega)](c) = \int_c \omega \quad (89)$$

for $\omega \in C^p(U)$ and all $c \in C_p(\mathcal{K})$. Here, ϕ^p makes a continuous field ω discretized. Now, we obtain a commutative diagram:

$$\begin{array}{ccccc} C^0(U) & \xrightarrow{d} & C^1(U) & \xrightarrow{d} & C^2(U) \\ \downarrow \phi^0 & & \downarrow \phi^1 & & \downarrow \phi^2 \\ C^0(\mathcal{K}) & \xrightarrow{d} & C^1(\mathcal{K}) & \xrightarrow{d} & C^2(\mathcal{K}) \end{array} \quad (90)$$

Commutativity can be checked as follows. We can calculate for all $f \in C^0(U)$, $c \in C_1(\mathcal{K})$ as

$$[\phi^1(df)](c) = \int_c df = \int_{\partial c} f = [\phi^0(f)](\partial c) = [d\phi^0(f)](c), \quad (91)$$

where we used Stokes' theorem. Similarly, we obtain $\phi^2(d\alpha) = d[\phi^1(\alpha)]$, for all $\alpha \in C^1(U)$. The commutative diagram of Equation (90) indicates that the discretization by ϕ keeps the algebraic structure of d .

Using ϕ , we can discretize an electric field (untwisted 1-form) E as $V = \sum_{i=1}^{|\mathcal{E}|} V_i e^i$ with $V_i = \int_{e_i} E$. Moreover, KVL ($dE = 0$) is discretized as

$$dV = 0, \tag{92}$$

which is explicitly expressed as $\sum_{j=1}^{|\mathcal{E}|} V_j \Pi^j_i = 0$. Therefore, Π^j_i represents the discretized rotation of the field.

For a current density K (twisted 1-form), we should consider the integration on the dual lattice. The set of all twisted p -forms on U is represented as $\check{C}^p(U)$. We have

$$[\check{\phi}^p(\check{\omega})](\check{\epsilon}) = \int_{\check{\epsilon}} \check{\omega} \tag{93}$$

for $\check{\omega} \in \check{C}^p(U)$ and all $\check{\epsilon} \in C_p(\mathcal{K}^*)$. Then, another diagram similar to Equation (90) is obtained:

$$\begin{array}{ccccc} \check{C}^0(U) & \xrightarrow{d} & \check{C}^1(U) & \xrightarrow{d} & \check{C}^2(U) \\ \downarrow \check{\phi}^0 & & \downarrow \check{\phi}^1 & & \downarrow \check{\phi}^2 \\ C^0(\mathcal{K}^*) & \xrightarrow{d} & C^1(\mathcal{K}^*) & \xrightarrow{d} & C^2(\mathcal{K}^*) \end{array} \tag{94}$$

Remembering $(\star_1)^{-1} : C^1(\mathcal{K}^*) \rightarrow C_1(\mathcal{K})$, we can define $I = (\star_1)^{-1}(\check{\phi}^1(K)) = \sum_{i=1}^{|\mathcal{E}|} I^i e_i$ with $I^i = \int_{\check{\epsilon}_i} K = \int_{(\star_1)^{-1}e^i} K$. Now, the discretized KCL is obtained as

$$\partial I = 0, \tag{95}$$

for which component representation is $\sum_{j=1}^{|\mathcal{E}|} \Delta^i_j I^j = 0$. Therefore, Δ^i_j indicates the discretized minus divergence.

For the discretization of Ohm's law, we interpolate E from E_i as

$$E \approx \sum_{i=1}^{|\mathcal{E}|} E_i w_{e_i}, \tag{96}$$

where $\{w_{e_i}\}$ are called interpolation forms. As the interpolation forms $\{w_{e_i}\}$, so-called Whitney forms can be used [62,79–82]. Now, Ohm's law is discretized as

$$I^i = \sum_{j=1}^{|\mathcal{E}|} \left(\int_{\check{\epsilon}_i} G \star w_{e_j} \right) E_j. \tag{97}$$

■ Correspondence between Keller–Dykhne Duality and Circuit Duality

Now, we establish correspondence between Keller–Dykhne duality and circuit duality. These two dualities are related through the diagram shown in Figure 35. In this section, we prove the commutativity of the two paths (1) and (2) in the figure.

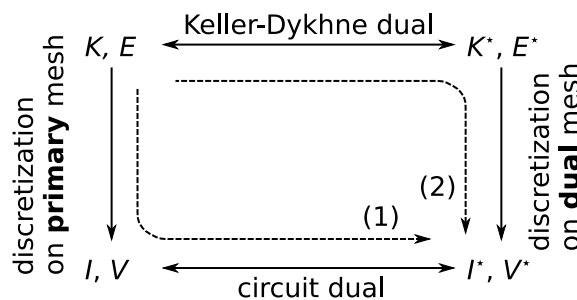


Figure 35. Relation between Keller–Dykhne duality and circuit duality.

- (1) For I and V discretized from K and E , we can consider the dual circuit with current $I^* := G_{\text{ref}}(\star^1)^{-1}(V)$ and voltage $V^* := R_{\text{ref}} \star_1(I)$ distributions for a circuit on \mathcal{K}^* :

$$I^* = G_{\text{ref}} \sum_{i=1}^{|\mathcal{E}|} V_i (\star^1)^{-1}(e^i) = G_{\text{ref}} \sum_{i=1}^{|\mathcal{E}|} V_i \check{e}_i, \tag{98}$$

$$V^* = R_{\text{ref}} \sum_{i=1}^{|\mathcal{E}|} I^i \star_1(e_i) = R_{\text{ref}} \sum_{i=1}^{|\mathcal{E}|} I^i \check{e}^i. \tag{99}$$

- (2) On the other hand, we discretize $E^* = R_{\text{ref}} K_\omega$ and $K^* = -G_{\text{ref}} \Omega^\omega E$ in a dual mesh \mathcal{K}^* . We need to choose a specific orientation ω of the plane, and $(\check{e}_i)_\omega$ is regarded as an inner-oriented edge in \mathcal{K}^* . Here, we introduce the \star -conjugate operation to give an outer-oriented dual edge as $e_i^* = \check{e}_i$. The dual edge $(\check{e}_i)_\omega^*$ is outer-oriented, and represented as $((\check{e}_i)_\omega^*)_\omega = -e_i$ (Figure 36), which reflects the complex algebraic structure of the plane. Then, discretized E^* and K^* are given as

$$\left(\int_{(\check{e}_i)_\omega} E^* \right) (\check{e}^i)_\omega = R_{\text{ref}} \left(\int_{\check{e}_i} K \right) (\check{e}^i)_\omega = (V^*)_\omega, \tag{100}$$

$$\left(\int_{(\check{e}_i)_\omega^*} K^* \right) (\check{e}_i)_\omega = \left(\int_{-e_i} (K^*)_\omega \right) (\check{e}_i)_\omega = G_{\text{ref}} \left(\int_{e_i} E \right) (\check{e}_i)_\omega = (I^*)_\omega. \tag{101}$$

These equations indicate the commutativity of the diagram shown in Figure 35. Thus, Keller–Dykhne duality corresponds to circuit duality through discretization.

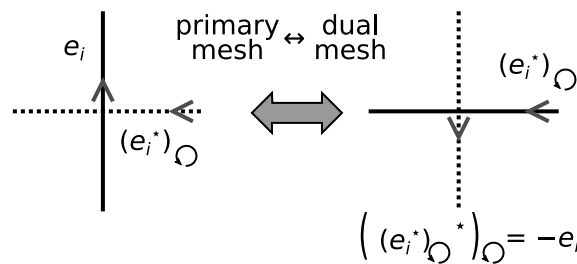


Figure 36. Interchange between a primary mesh and dual mesh.

5. Electromagnetic Duality

The electric field induced by an electric dipole has similar properties to the magnetic field created by a magnetic dipole. Such similarities can be considered as an emergent form of *electromagnetic duality*. To correctly understand electromagnetic duality, we need to clarify the difference between electric and magnetic fields. To this end, we utilize inner- and outer-oriented vectors called *polar* and *axial* vectors, respectively [78]. By using these concepts, we accurately formulate electromagnetic duality, while the role of orientation of the space in electromagnetic duality is elucidated. The analogy between electromagnetic duality and Keller–Dykhne duality is also discussed.

5.1. Preliminary

■ Polar and Axial Vectors

Here, we introduce two different kinds of vectors. Consider a line segment in a three-dimensional space. As discussed in Section 2.3, we can set an inner or outer orientation of the line. An inner-oriented line is called a *polar vector* and is represented by an arrow depicted in Figure 37a. The totality of polar vectors forms a vector space, in which we define the sum of vectors and scalar multiplication of a vector. An electric field is represented by a polar-vector field. On the other hand, an outer-oriented line can be considered as shown in Figure 37b. Such an outer-oriented line segment is called an *axial*

vector. Axial vectors also form a vector space. As we saw in Section 2.3, an outer-oriented object can be represented by two-different inner-oriented ones. Here, we can represent the orientation of the space by a helix, of which the winding direction is right- or left-handed. The helix winding direction is arranged to be the same as the outer orientation of the axial vector, then the advance direction of the corresponding screw induces the inner orientation of the line as shown in Figure 38. In other words, when fingers of the left or right hand representing the helix handedness are curled in the direction of the outer orientation, the thumb points out the inner orientation. Then, an axial vector is denoted by $\mathbf{a} = \{\mathbf{a}_o | o \in \mathcal{O}\}$ with polar vectors satisfying $\mathbf{a}_{-o} = -\mathbf{a}_o$ for the set \mathcal{O} of two spatial orientations. Importantly, an axial vector is a geometric object independent of the orientation of the space, although the polar vector obtained from the axial vector depends on the spatial orientation.

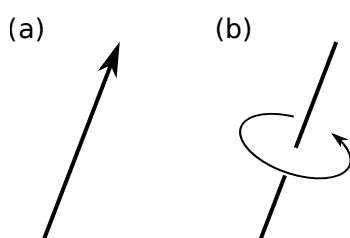


Figure 37. (a) polar vector; (b) axial vector.

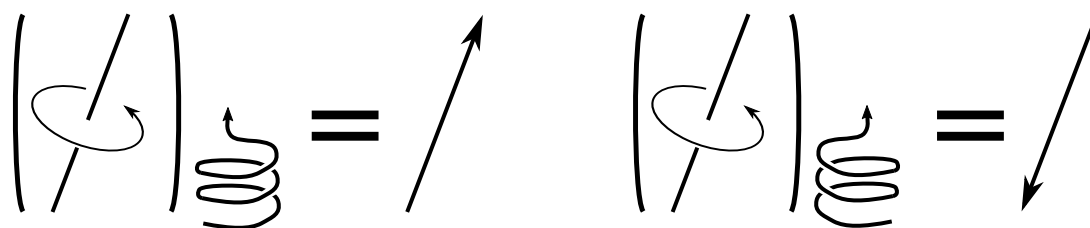


Figure 38. Representation of an axial vector by polar vectors depending on the space orientation. A spatial orientation is entered in the subscript position and its output is a polar vector which depends on the spatial orientation.

■ Magnetic Field as Axial Vectors

To explain the necessity of the axial vectors, we consider Ampère’s law. The conventional image of a magnetic field induced by a current flowing along a line ($x = y = 0$) is depicted in Figure 39a, where the direction of the magnetic field is determined by the so-called right-hand rule. However, there are three unnatural points in this illustration: (i) Why is the right-hand rule required? (ii) Mirror reflection with respect to $x = 0$ or $y = 0$ does not change the current flow, but it alters the direction of the vector field. Here, mirror reflection \mathcal{M}_x with respect to $x = 0$ operates as $[\mathcal{M}_x \mathbf{v}](x, y, z) = -v^x(-x, y, z)\mathbf{e}_x + v^y(-x, y, z)\mathbf{e}_y + v^z(-x, y, z)\mathbf{e}_z$ for a polar vector field $\mathbf{v}(x, y, z) = v^x(x, y, z)\mathbf{e}_x + v^y(x, y, z)\mathbf{e}_y + v^z(x, y, z)\mathbf{e}_z$. (iii) Mirror reflection with respect to $z = 0$ changes the direction of the current, but the vector field is unchanged under the operation. These three problems are resolved when we consider magnetic fields as axial vector fields. A proper illustration of the magnetic field is shown in Figure 39b, where the magnetic line is outer-oriented. In this representation, we do not need the right-hand rule. The field in Figure 39b is symmetric with respect to $x = 0$ or $y = 0$, while it is antisymmetric with respect to $z = 0$. Figure 39a is now interpreted as the right-hand component for Figure 39b.

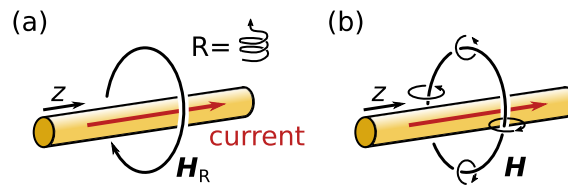


Figure 39. Ampère's law represented by (a) polar and (b) axial magnetic lines.

■ Vector Product

Another important operation that can generate an axial vector is the vector product of polar vectors. Consider the vector product between polar vectors A and B . Clearly, A and B are invariant under a mirror reflection with respect to the plane spanned by A and B . Therefore, it is natural to consider $A \times B$ as an axial vector as shown in Figure 40a. Then, the mirror symmetry is kept. The representation by polar vectors is also depicted in Figure 40b. The vector product between a polar vector and an axial vector is also defined to give a polar vector.

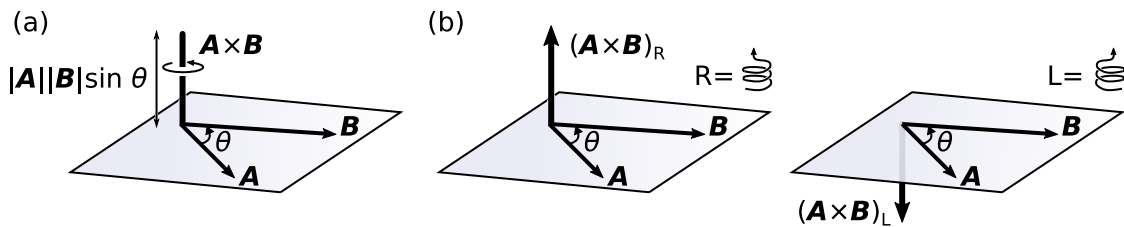


Figure 40. (a) axial vector obtained from a vector product of polar vectors; (b) its polar-vector representation.

■ Scalar and Pseudoscalar

For a scalar, we can consider an outer-oriented object. The codimension for a scalar is three in this three-dimensional space. Therefore, an outer-oriented or twisted scalar can be represented by a helix in this space. An outer-oriented scalar is often called a pseudoscalar. A pseudoscalar \check{s} is represented by two scalars $\check{s} = \{\check{s}_o | o \in \mathcal{O}\}$ with $\check{s}_{-o} = -\check{s}_o$.

For example, magnetic charge density $\rho_m = \nabla \cdot B$ is a pseudoscalar because magnetic flux density B is an axial vector. Therefore, a magnetic charge should be a pseudoscalar if it exists. The difference between electric and magnetic charges is illustrated in Figure 41.

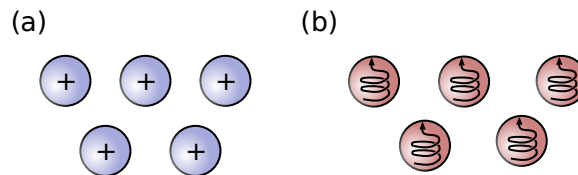


Figure 41. (a) electric charges as a scalar; (b) magnetic charges as a pseudoscalar.

5.2. Formulation of Electromagnetic Duality

■ Maxwell's Equations

Maxwell's equations can be written as

$$\nabla \times E + \frac{\partial B}{\partial t} = -J_m, \quad \nabla \cdot D = \rho_e \tag{102}$$

$$\nabla \times H - \frac{\partial D}{\partial t} = J_e, \quad \nabla \cdot B = \rho_m \tag{103}$$

with electric field E , electric displacement field D , electric current density J_e , electric charge density ρ_e , magnetic field H , magnetic flux density B , magnetic current density J_m , and magnetic charge density ρ_m . While E , D , and J are polar vectors, H , B , and J_m are axial vectors. Electric and magnetic charge densities are represented by a scalar and pseudoscalar, respectively. Here, we introduce J_m and ρ_m to investigate the duality. Note that J_m and ρ_m are fictitious because a magnetic monopole does not exist. Material fields (D , H) are determined from (E , B) through the constitutive equations as described later.

■ Electromagnetic Duality Transformation

Electric and magnetic fields are represented by polar and axial vectors as shown in Figure 37, respectively. To exchange these two different types of vectors, we need to fix the orientation of the space to σ and introduce a pseudoscalar Ω^σ as $(\Omega^\sigma)_\sigma = +1$ and $(\Omega^\sigma)_{-\sigma} = -1$. The pseudoscalar Ω^σ can be represented by a helix with winding of σ as shown in Figure 42. For an axial vector a , Ω^σ converts it to the polar component as $\Omega^\sigma a = a_\sigma$.

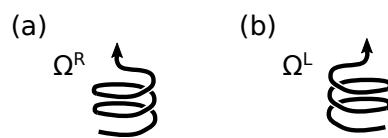


Figure 42. (a) Ω^R and (b) Ω^L .

We set a reference resistance $R_{\text{ref}} (= 1/G_{\text{ref}})$. For a spatial orientation σ , the electromagnetic duality transformation is given by

$$\mathbf{E}^* = R_{\text{ref}} \Omega^\sigma \mathbf{H}, \quad \mathbf{D}^* = G_{\text{ref}} \Omega^\sigma \mathbf{B}, \quad (104)$$

$$\mathbf{H}^* = -G_{\text{ref}} \Omega^\sigma \mathbf{E}, \quad \mathbf{B}^* = -R_{\text{ref}} \Omega^\sigma \mathbf{D}. \quad (105)$$

Under the duality transformation, Maxwell's equations are invariant as

$$\nabla \times \mathbf{E}^* + \frac{\partial \mathbf{B}^*}{\partial t} = -\mathbf{J}_m^*, \quad \nabla \cdot \mathbf{D}^* = \rho_e^*, \quad (106)$$

$$\nabla \times \mathbf{H}^* - \frac{\partial \mathbf{D}^*}{\partial t} = \mathbf{J}_e^*, \quad \nabla \cdot \mathbf{B}^* = \rho_m^* \quad (107)$$

with

$$\rho_e^* = G_{\text{ref}} \Omega^\sigma \rho_m, \quad \mathbf{J}_e^* = G_{\text{ref}} \Omega^\sigma \mathbf{J}_m, \quad (108)$$

$$\rho_m^* = -R_{\text{ref}} \Omega^\sigma \rho_e, \quad \mathbf{J}_m^* = -R_{\text{ref}} \Omega^\sigma \mathbf{J}_e. \quad (109)$$

■ Duality for Constitutive Equations

Consider the relations called constitutive equations

$$\mathbf{D} = \varepsilon \mathbf{E} + \zeta \mathbf{H}, \quad (110)$$

$$\mathbf{B} = \zeta \mathbf{E} + \mu \mathbf{H}, \quad (111)$$

where ζ and ζ are twisted. Generally, ε , ζ , ζ , and μ are tensors. Under Equations (104) and (105), the constitutive equations are transformed as

$$\mathbf{D}^* = \varepsilon^* \mathbf{E}^* + \zeta^* \mathbf{H}^*, \quad (112)$$

$$\mathbf{B}^* = \zeta^* \mathbf{E}^* + \mu^* \mathbf{H}^* \quad (113)$$

with

$$\varepsilon^* = (G_{\text{ref}})^2 \mu, \quad \zeta^* = -\zeta, \quad (114)$$

$$\zeta^* = -\zeta, \quad \mu^* = (R_{\text{ref}})^2 \varepsilon. \quad (115)$$

■ Self-Dual Media

Now, we require the set of self-dual conditions $\varepsilon^* = \varepsilon$, $\zeta^* = \zeta$, $\mu^* = \mu$, and $\zeta^* = \zeta$. Then, the following equations should hold:

$$\varepsilon = (G_{\text{ref}})^2 \mu, \quad \zeta = -\zeta. \quad (116)$$

Here, the G_{ref} satisfying Equation (116) is called the admittance Y of the medium. For scalar ε and μ , we have $Y = \sqrt{\varepsilon/\mu}$. In particular, a vacuum with $\varepsilon = \varepsilon_0$, $\mu = \mu_0$, $\zeta = \zeta = 0$ is self-dual with respect to the vacuum admittance $Y_0 = \sqrt{\varepsilon_0/\mu_0}$. In circuit theory, a self-dual system did not have backscattering. This statement is also established in electromagnetic systems under certain conditions [54]. In addition, the duality transformation can be extended to continuous one and continuous self-dual symmetry leads to the helicity conservation law [55,83–88].

5.3. Analogy between Keller–Dykhne Duality and Electromagnetic Duality

Maxwell's electromagnetic theory in a four-dimensional spacetime has an analogous structure to the sheet problem discussed in Section 4. To see this analogy, we use the differential-form approach to Maxwell's equations [62,89–92]. The wedge product, exterior derivative, integral, and Hodge star are naturally extended in dimensions greater than two.

In a three-dimensional space, an electric field and magnetic field are represented by an untwisted 1-form E and twisted 1-form H , respectively. On the other hand, a magnetic flux density is denoted by an untwisted 2-form B , while an electric displacement is represented by a twisted 2-form D . Using these quantities, we define untwisted and twisted 2-forms F and G as

$$F = E \wedge dt + B, \quad (117)$$

$$G = -H \wedge dt + D, \quad (118)$$

respectively. Maxwell's equations without a source are equivalent to

$$dF = 0, \quad (119)$$

$$dG = 0, \quad (120)$$

with the four-dimensional exterior derivative d . Now, we consider a medium with a scalar permittivity ε and permeability μ , while we set $\zeta = 0$ and $\zeta = 0$. The constitutive equation is given by

$$G = Y \star F \quad (121)$$

with the admittance $Y = \sqrt{\varepsilon/\mu}$ ($= 1/Z$) and the four-dimensional Hodge star operator \star . These equations are summarized in Figure 43. For 2-forms in the four-dimensional space, we have

$$\star \star = -\text{Id}, \quad (122)$$

with the identity operator Id . Equation (122) leads to a complex structure.

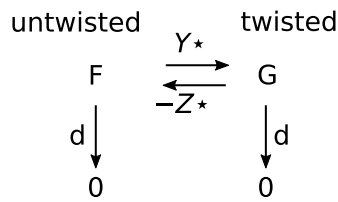


Figure 43. Structure of Maxwell’s theory of electromagnetism.

Equations (119)–(121) perfectly correspond to Equations (79)–(81), respectively. When we fix an orientation ω of the four-dimensional spacetime, the duality transformation can be written as

$$F^* = -R_{\text{ref}}\Omega^\omega G, \tag{123}$$

$$G^* = G_{\text{ref}}\Omega^\omega F. \tag{124}$$

Then, the dual admittance is defined as

$$Y^* = (G_{\text{ref}})^2/Y. \tag{125}$$

The duality transformation of Equations (123) and (124) interchanges E and H in the three-dimensional space. If we set $G_{\text{ref}} = Y$, we obtain $Y^* = Y$, which indicates the system is self-dual. As an example, a vacuum is self-dual with respect to the vacuum admittance $Y_0 = \sqrt{\epsilon_0/\mu_0}$ ($= 1/Z_0$) with vacuum permittivity ϵ_0 and vacuum permeability μ_0 . Electromagnetic duality can be considered as a manifestation of Poincaré duality in this spacetime [93].

6. Babinet Duality

Babinet’s principle known in optics and electromagnetism relates wave-scattering problems of two complementary screens (Figure 44) [94]. Here, we call the duality appearing in Babinet’s principle as *Babinet duality*. Babinet duality can be regarded as a high-frequency counterpart of Keller–Dykhne duality, which is discussed in Section 4. At first, we introduce rigorous Babinet’s principle for electromagnetic waves. Then, we analyze self-dual systems in terms of Babinet duality, such as the Mushiake principle in antenna theory [13]. Finally, we discuss Babinet duality in the light of circuit duality by using a transmission-line model of metasurfaces.

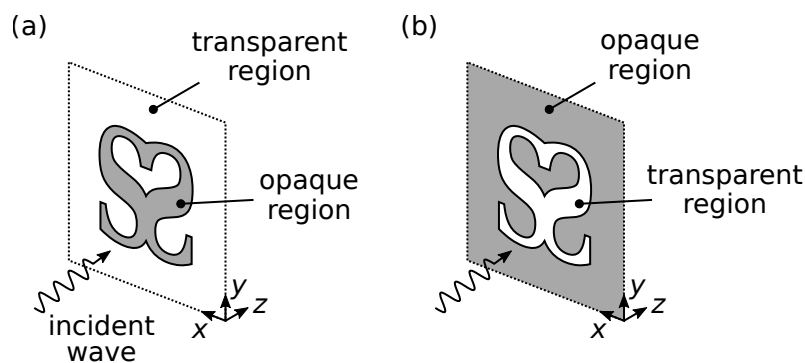


Figure 44. (a,b) two scattering problems that are dual with each other. Opaque and transparent regions are interchanged under the duality transformation. The screen in (b) is called the complementary screen of that in (a), and vice versa.

6.1. Babinet’s Principle for Electromagnetic Waves

Before moving on to Babinet’s principle for electromagnetic waves, we discuss the duality for electromagnetic waves radiated from planar sheets. Next, the formulated duality is utilized to derive Babinet’s principle for electromagnetic waves.

■ Duality for Radiation from Planar Antennas

Here, we formulate the duality for fields radiated from nonuniform planar sheets in a vacuum, while we stress the importance of axial vectors. Consider a sheet on $z = 0$ with an electric sheet impedance $Z_e(x, y)$ and an external electric field $\tilde{\mathbf{E}}_{\text{ext}}(x, y)$ as a voltage source. Generally, $Z_e(x, y)$ is a tensor. Following Maxwell’s equations, the induced current distribution radiates electromagnetic waves. The radiated electromagnetic field is represented by $(\tilde{\mathbf{E}}_+, \tilde{\mathbf{H}}_+)$ and $(\tilde{\mathbf{E}}_-, \tilde{\mathbf{H}}_-)$ in $z \geq 0$ and $z \leq 0$, respectively. Mirror reflection with respect to $z = 0$ is expressed as \mathcal{M}_z and the considered system is invariant under \mathcal{M}_z . First, let us see the symmetry property of electromagnetic fields on $z = 0$. The component of \mathbf{v} perpendicular to the plane $z = 0$ is obtained by $\mathbf{v}_n = (\mathbf{v} \cdot \mathbf{e}_z)\mathbf{e}_z$. Then, the projection of \mathbf{v} onto $z = 0$ is given by $\mathbf{v}_t = \mathcal{P}\mathbf{v} = \mathbf{v} - \mathbf{v}_n$ with $\mathcal{P} = -\mathbf{e}_z \times \mathbf{e}_z \times$. A polar vector \mathbf{p} and axial vector \mathbf{a} behave differently for \mathcal{M}_z as

$$\mathcal{M}_z \mathbf{p} = \mathbf{p}_t - \mathbf{p}_n \tag{126}$$

$$\mathcal{M}_z \mathbf{a} = -\mathbf{a}_t + \mathbf{a}_n. \tag{127}$$

These relations are schematically shown in Figure 45. From Equations (126) and (127), we obtain the following symmetry at any point of the plane $z = 0$:

$$\mathcal{P}\tilde{\mathbf{E}}_+ = \mathcal{P}\tilde{\mathbf{E}}_-, \quad \mathbf{e}_z \cdot \tilde{\mathbf{E}}_+ = -\mathbf{e}_z \cdot \tilde{\mathbf{E}}_-, \tag{128}$$

$$\mathcal{P}\tilde{\mathbf{H}}_+ = -\mathcal{P}\tilde{\mathbf{H}}_-, \quad \mathbf{e}_z \cdot \tilde{\mathbf{H}}_+ = \mathbf{e}_z \cdot \tilde{\mathbf{H}}_-. \tag{129}$$

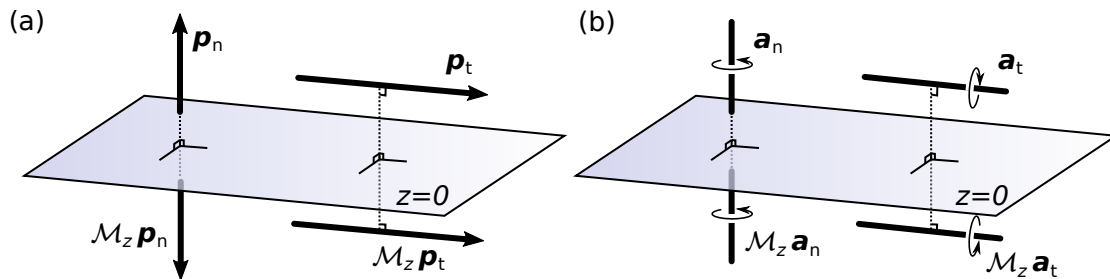


Figure 45. Mirror reflection of (a) polar and (b) axial vectors.

Next, the boundary condition on $z = 0$ is given by

$$\mathcal{P}\tilde{\mathbf{E}}_+ = \mathcal{P}\tilde{\mathbf{E}}_-, \tag{130}$$

$$\tilde{\mathbf{E}}_{2D} = \mathcal{P}(\tilde{\mathbf{E}}_+ + \tilde{\mathbf{E}}_{\text{ext}}) = Z_e \tilde{\mathbf{K}}_{2D}, \tag{131}$$

with the two-dimensional electric field $\tilde{\mathbf{E}}_{2D}$ on $z = 0$, the sheet current density $\tilde{\mathbf{K}}_{2D} = \mathbf{e}_z \times (\tilde{\mathbf{H}}_+ - \tilde{\mathbf{H}}_-) = 2\mathbf{e}_z \times \tilde{\mathbf{H}}_+$ which is obtained from Equation (129). Equation (130) represents the continuity of the tangential electric field, while Equation (131) is equivalent to Ohm’s law. The boundary conditions for $\tilde{\mathbf{D}}$ and $\tilde{\mathbf{H}}$ are derived from these boundary conditions [95].

Finally, we consider the duality transformation. We fix a spatial orientation σ and introduce a pseudoscalar Ω^σ satisfying $(\Omega^\sigma)_\sigma = 1$ and $(\Omega^\sigma)_{-\sigma} = -1$. The following duality transformations are considered:

1. $z \geq 0$:

$$\tilde{\mathbf{E}}_+^* = -Z_0 \Omega^\sigma \tilde{\mathbf{H}}_+, \quad \tilde{\mathbf{H}}_+^* = Y_0 \Omega^\sigma \tilde{\mathbf{E}}_+, \tag{132}$$

2. $z \leq 0$:

$$\tilde{\mathbf{E}}_-^* = Z_0 \Omega^\sigma \tilde{\mathbf{H}}_-, \quad \tilde{\mathbf{H}}_-^* = -Y_0 \Omega^\sigma \tilde{\mathbf{E}}_-, \tag{133}$$

where $Z_0 (= 1/Y_0)$ is the impedance of a vacuum. The transformed fields $(\tilde{\mathbf{E}}_\pm^*, \tilde{\mathbf{H}}_\pm^*)$ are invariant under \mathcal{M}_z as shown in Figure 46. With this symmetry of Equation (129), we immediately obtain $\mathcal{P}\tilde{\mathbf{E}}_+^* = \mathcal{P}\tilde{\mathbf{E}}_-^*$ on $z = 0$. On the other hand, Equation (131) is transformed as

$$\tilde{\mathbf{K}}_{2D}^* = Y_e^* \tilde{\mathbf{E}}_{2D}^*, \tag{134}$$

where we defined

$$\tilde{\mathbf{K}}_{2D}^* = 2\mathbf{e}_z \times \tilde{\mathbf{H}}_+^* + \tilde{\mathbf{K}}_{\text{ext}}^* \tag{135}$$

$$\tilde{\mathbf{K}}_{\text{ext}}^* = 2Y_0 \Omega^\sigma \mathbf{e}_z \times \tilde{\mathbf{E}}_{\text{ext}} \tag{136}$$

with $Z_e^* = (Y_e^*)^{-1}$. Here, the following general impedance inversion holds:

$$Z_e^* J Z_e J^{-1} = \left(\frac{Z_0}{2}\right)^2 \tag{137}$$

with

$$J = \begin{bmatrix} 0 & -1 \\ 1 & 0 \end{bmatrix}.$$

Note that the impedance Z_0 can be replaced with $\sqrt{\mu/\epsilon}$ if the screen is placed in an isotropic and homogeneous medium with permeability μ and permittivity ϵ . Furthermore, $\tilde{\mathbf{E}}_{2D}^* = \mathcal{P}\tilde{\mathbf{E}}_+^*$ and $\tilde{\mathbf{K}}_{2D}^*$ satisfy

$$\tilde{\mathbf{E}}_{2D}^* = \frac{Z_0}{2} \Omega^\sigma \mathbf{e}_z \times \tilde{\mathbf{K}}_{2D}, \tag{138}$$

$$\tilde{\mathbf{K}}_{2D}^* = \left(\frac{Z_0}{2}\right)^{-1} \Omega^\sigma \mathbf{e}_z \times \tilde{\mathbf{E}}_{2D} \tag{139}$$

on $z = 0$. Equations (137), (138), and (139) perfectly correspond to Equations (49), (43), and (44). For the dual setup with the sheet impedance Z_e^* and current source $\tilde{\mathbf{K}}_{\text{ext}}^*$, the radiated fields are given by $(\tilde{\mathbf{E}}_\pm^*, \tilde{\mathbf{H}}_\pm^*)$. For a scalar Z_e , the impedance inversion simplifies to

$$Z_e Z_e^* = \left(\frac{Z_0}{2}\right)^2. \tag{140}$$

Note that Equation (140) includes the duality between the perfect electric conductor ($Z_e = 0$) and aperture ($Z_e = \infty$). In other words, the sheet-impedance model is a generalization of the binarized case, where only opaque and transparent regions were considered for screens as shown in Figure 44.

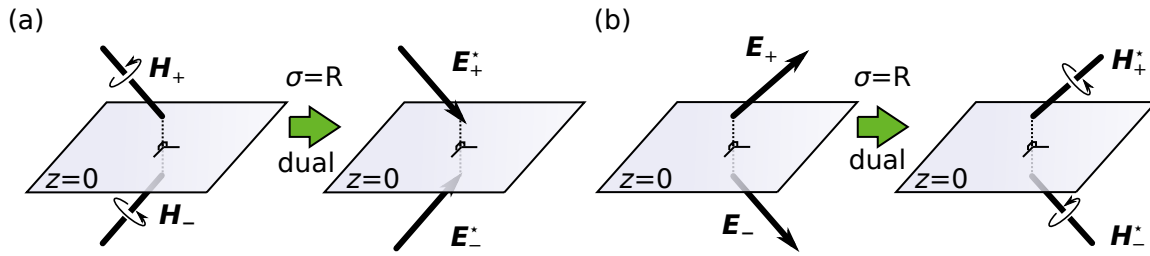


Figure 46. Duality transformation keeping the mirror symmetry. (a) H_{\pm} to E_{\pm}^* and (b) E_{\pm} to H_{\pm}^* .

■ Babinet’s Principle for Sheet-Impedance Screens

Here, we derive Babinet’s principle by applying the previous discussion to scattering problems. We consider a scattering problem by a screen characterized with a sheet impedance of $Z_e(x, y)$ for an incident electromagnetic field $(\tilde{E}_{in}, \tilde{H}_{in})$ from $z < 0$, as shown in Figure 47a. Fields scattered by the screen are denoted by $(\tilde{E}_{s,\pm}, \tilde{H}_{s,\pm})$ for $z \geq 0$ and $z \leq 0$, respectively. These scattered fields are induced by the external electric field $\tilde{E}_{ext} = \mathcal{P}\tilde{E}_{in}(x, y, 0)$ on $z = 0$.

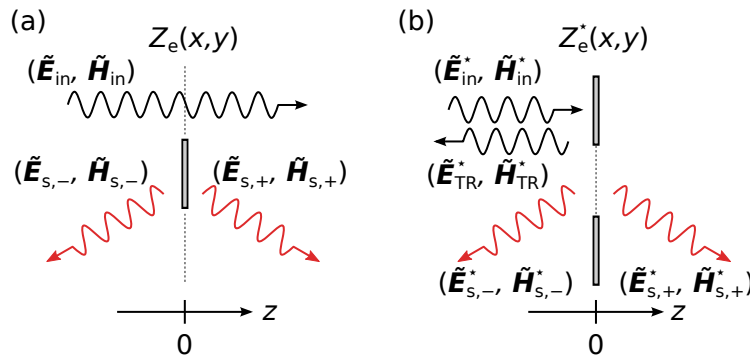


Figure 47. (a,b) two scattering problems that are dual with each other. The dual screen (b) is obtained through the impedance inversion of Equation (137).

Next, we consider the dual wave scattering by $Z_e^*(x, y)$ for an incident wave

$$(\tilde{E}_{in}^*, \tilde{H}_{in}^*) = (Z_0 \Omega^\sigma \tilde{H}_{in}, -Y_0 \Omega^\sigma \tilde{E}_{in}), \tag{141}$$

from $z < 0$. In the dual problem, we have to inject an external current rather than apply an electric field. To this end, we virtually consider total reflection by a perfect electric conductor sheet at $z = 0$. The totally reflected field $(\tilde{E}_{TR}^*, \tilde{H}_{TR}^*)$ is obtained by a mirror reflection of $(\tilde{E}_{in}^*, \tilde{H}_{in}^*)$ in $z > 0$ with respect to $z = 0$ and a phase flip:

$$(\tilde{E}_{TR}^*, \tilde{H}_{TR}^*) = -(\mathcal{M}_z \tilde{E}_{in}^*, \mathcal{M}_z \tilde{H}_{in}^*). \tag{142}$$

Using the total reflection, we can introduce an external current as

$$\tilde{K}_{ext}^* = -2e_z \times \tilde{H}_{in}^* = 2Y_0 \Omega^\sigma e_z \times \tilde{E}_{ext} \tag{143}$$

on $z = 0$. This virtually injected current radiates the electromagnetic field $(\tilde{E}_{s,\pm}^*, \tilde{H}_{s,\pm}^*)$ as shown in Figure 47b. Here, Equation (143) is identical to Equation (136). Therefore, $(\tilde{E}_{s,\pm}, \tilde{H}_{s,\pm})$ and $(\tilde{E}_{s,\pm}^*, \tilde{H}_{s,\pm}^*)$ are related through Equations (132) and (133), if Z_e^* satisfies Equation (137). Thus, we could relate the scattered fields in the two problems. This duality relationship is the Babinet’s principle for vector waves.

Babinet’s principle leads to complementary relation on transmission coefficients. Consider a normal incidence of a plane wave to a periodic screen (metasurface) with a sheet impedance $Z_e(x, y)$

on $z = 0$. The complex transmission coefficient to the transmitting mode with the same polarization is denoted by τ . In the dual situation, the incident wave of Equation (141) enters the dual metasurface $Z_e^*(x, y)$ satisfying Equation (137). The complex electric transmission coefficient in the dual setup is represented by τ^* . Now, the following dual relation holds:

$$\tau + \tau^* = 1. \quad (144)$$

The detailed derivation of this relation is given in Appendix B.

■ Babinet's Principle for Power Transmissions

Next, we consider the consequence of Babinet duality on power transmission spectra of periodic screens, i.e., the square of the absolute value of the complex amplitude transmission coefficients. Using the continuity equation $1 + \rho = \tau$ with a reflection coefficient ρ , we obtain

$$\rho = -\tau^*. \quad (145)$$

On the other hand, we have the energy-conservation relation

$$|\tau|^2 + |\rho|^2 = 1, \quad (146)$$

under the following conditions: (i) periodicity of screens is smaller than the wavelength and thus energy scattering into the other diffraction modes except for the zeroth order modes is negligible, and (ii) polarization conversion is negligible ($\tau^\perp = \rho^\perp = 0$ in Appendix B). By using Equations (145) and (146), we obtain

$$|\tau|^2 + |\tau^*|^2 = 1. \quad (147)$$

This equation indicates that the power transmission spectrum in the dual problem has the opposite shape of that in the original one.

6.2. Self-Dual Systems in Terms of Babinet Duality

In this subsection, we discuss the manifestation of self-duality in terms of Babinet duality. First, we introduce self-complementary antennas, and then we discuss the criticality of metallic checkerboard-like metasurfaces.

■ Self-Complementary Antennas

In antenna theory, it is well-known that antennas with self-complementary geometry show a frequency-independent input impedance, which is defined as the ratio of voltage and current at a feeding point of an antenna, and such antennas are called self-complementary antennas [13].

Before moving on to the self-complementary case, we introduce duality for the effective response of antennas. Consider an antenna with an electric sheet admittance $Y_e(x, y) (= Z_e(x, y)^{-1})$ on $z = 0$ as shown in Figure 48a. On a rectangular patch S , an external voltage distribution $\tilde{E}_{\text{ext}}(x, y)$ is applied. We assume that \tilde{E}_{ext} is directed in the y -direction. For the dual setup, we set Z_e^* satisfying Equation (137) and an external current $\tilde{K}_{\text{ext}}^* = 2Y_0\Omega^{\sigma} e_z \times \tilde{E}_{\text{ext}}$ on S in Figure 48b. In particular, when antennas are made only of perfect electric conductor ($Y_e = \infty$), the corresponding dual antennas have complementary shapes, which are obtained by interchanging metallic regions and hole regions. The input impedances of the original and dual antenna are denoted by Z_{in} and Z_{in}^* , respectively. From Babinet duality, these input impedances satisfy

$$Z_{\text{in}}Z_{\text{in}}^* = \left(\frac{Z_0}{2}\right)^2, \quad (148)$$

as derived in Appendix C. This equation means that the input impedance of the dual antenna is related to that of the original antenna.

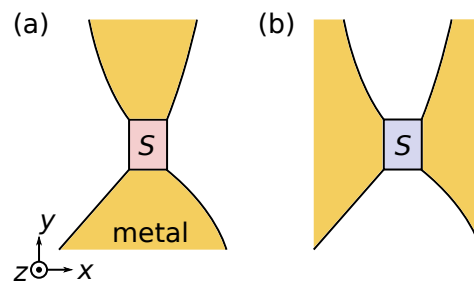


Figure 48. (a) antenna on $z = 0$ with voltage source on S ; (b) dual antenna with current source on S . Note that metallic and vacant regions are interchanged through the impedance inversion.

Now, we consider self-dual antennas. An example of a self-dual antenna is realized with a self-complementary geometry as shown in Figure 49. From Equation (148) and self-dual condition $Z_{in} = Z_{in}^*$, we obtain

$$Z_{in} = Z_{in}^* = \frac{Z_0}{2}, \quad (149)$$

and this means that the input impedance of self-complementary antennas is independent of frequency. Thus, the principle of self-complementary antennas called the “Mushlake Principle” [96] plays an important role in designing broadband antennas [13]. Because semi-infinite free spaces in $z > 0$ and $z < 0$ are seen as two parallel transmission lines with the characteristic impedance of Z_0 , Equation (149) shows that self-complementary antennas are perfectly matched to the composite impedance of $Z_0/2$.

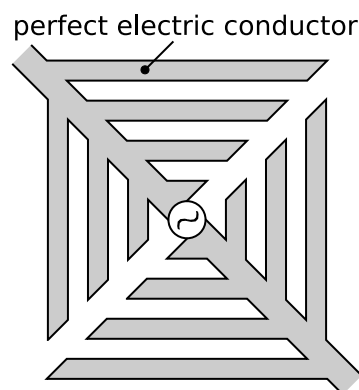


Figure 49. Example of a self-complementary antenna.

■ Critical Transition of Metallic Checkerboard-Like Metasurfaces

Here, we discuss critical behaviors of metallic checkerboard-like metasurfaces from the point of view of self-duality in Babinet duality. We assume the metasurfaces are placed in a vacuum and made of a perfect electric conductor. If we assume the periodicity of the checkerboard-like metasurfaces, we can classify them into three distinct cases as shown in Figure 50: (a) metallic patches are disconnected (disconnected phase), (b) metasurface is self-complementary, i.e., the metallic patches touch each other at ideal point contacts (self-complementary point), and (c) metallic patches are connected (connected phase). Note that structures in (c) are complementary to those in (a) if $w = w^*$; therefore, the two phases are related through Babinet duality. Now, consider the transition from the disconnected phase to the connected phase. Under this transition, the checkerboard-like metasurface passes through the self-complementary point between the two phases, as shown in Figure 50. As we

see below, the electromagnetic responses of checkerboard-like metasurfaces abruptly change at this self-complementary point, and this point is actually a *singular* point [44,45,47].

At first, we explain general transmission properties of checkerboard-like metasurfaces. We consider that a circularly polarized plane wave with wavevector $\mathbf{k} = k\mathbf{e}_z$ is normally incident on the metasurfaces, and we observe the transmission behind the metasurfaces. For the disconnected phase shown in Figure 50a, the power-transmission spectrum is typically like the lower panel of Figure 50a. The metasurfaces in the disconnected phase behave as capacitive filters, which highly transmit lower frequency components, while they resonantly reflect around the higher resonance frequency [97]. Note that the incident frequency axis is clipped at the lowest diffraction frequency c_0/a , where a is the size of the unit cell of the metasurfaces. Above the lowest diffraction frequency, the incident energy is enabled to be transmitted into higher-order diffraction modes with $\mathbf{k} \neq \pm k\mathbf{e}_z$. In other words, effective loss (mode-conversion loss) appears for the zeroth-order mode. To restrict our discussion to the single mode, we consider frequencies below c_0/a in the following. In addition to this constraint, thanks to the 4-fold rotational symmetry of the metasurfaces, polarization conversion is prohibited ($\tau^\perp = \rho^\perp = 0$). Then, we can use Equation (147) to obtain the power-transmission spectrum of the complementary structures: $|\tau^*|^2 = 1 - |\tau|^2$. In other words, the connected phase shown in Figure 50c exhibits transmission spectra with the upside-down shapes to those of the disconnected phase: it highly reflects lower frequency components, while it resonantly transmits around the higher resonant frequency, as shown in the lower panel of Figure 50c [97].

Now, we derive the criticality of the self-complementary structure. At the self-complementary point shown in Figure 50b, we have

$$\tau = \tau^*, \quad (150)$$

from the self-duality of the problem. Combining above with Equations (144) and (145), we can derive

$$\tau = \tau^* = -\rho = \frac{1}{2}. \quad (151)$$

Then, it is concluded that the self-complementary metasurface shows a *finite dissipation* $A = 1 - |\tau|^2 - |\rho|^2 = 1/2$. The finite dissipation obviously contradicts the assumption that the system is made of a lossless perfect electric conductor. Note that this contradiction occurs below the diffraction frequency c_0/a . For frequencies above c_0/a , scattering into the diffraction modes is enabled, and thus A is composed of not only dissipation but also mode conversion. In addition to this contradiction, the frequency-independent behavior also contradicts Foster's reactance theorem, which states that the imaginary part of the impedance of a lossless and passive system must increase monotonically with the frequency [98]. Thus, the transmission spectra of such systems cannot be flat. Consequently, we can conclude that there is no physical solution for the ideal self-complementary point and thus the checkerboard-like metasurface at the self-complementary point is singular.

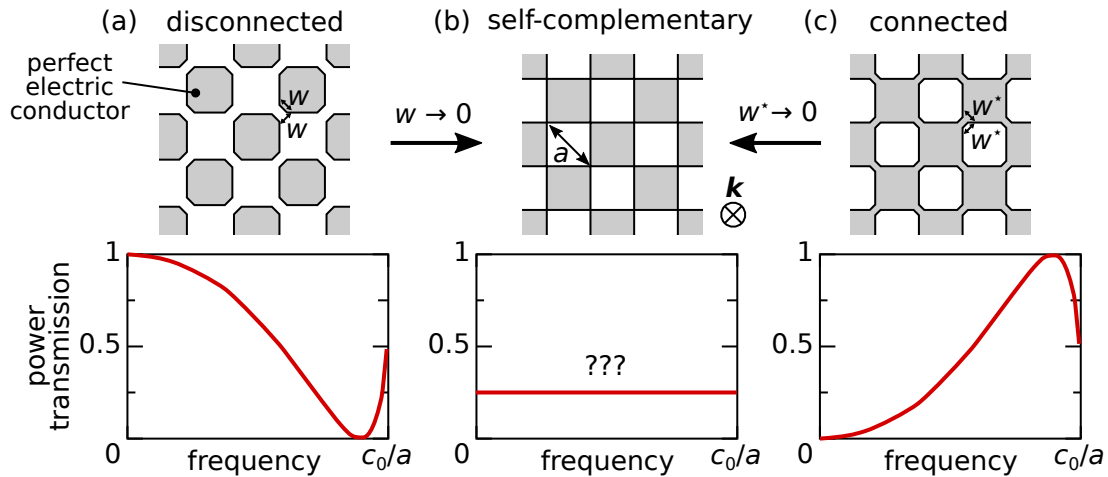


Figure 50. Metallic checkerboard-like metasurfaces and their typical power-transmission spectra. (a) disconnected phase; (b) self-complementary point; and (c) connected phase. The size of the unit cell is denoted by a .

Note that the *dissipative* intermediate structure in the transition between the disconnected and connected phases is physically consistent, although the *lossless* intermediate structure is singular. Such a dissipative intermediate structure, which contains dissipative elements (resistive sheets with sheet impedance of $Z_0/2$) at the connecting points of the checkerboard-like metasurfaces, can be characterized by the novel frequency-independent response with $\tau = -\rho = 1/2$ and dissipation $A = 1/2$ [37], as shown in Figure 51. The frequency-independent response has been experimentally observed in the terahertz frequency region [38]. In addition, introducing randomness into the connectivity of the metallic patches also leads to the similar flat spectrum [42,48]. In this random case, loss A results from mode conversion due to the randomness of the metasurface structure.

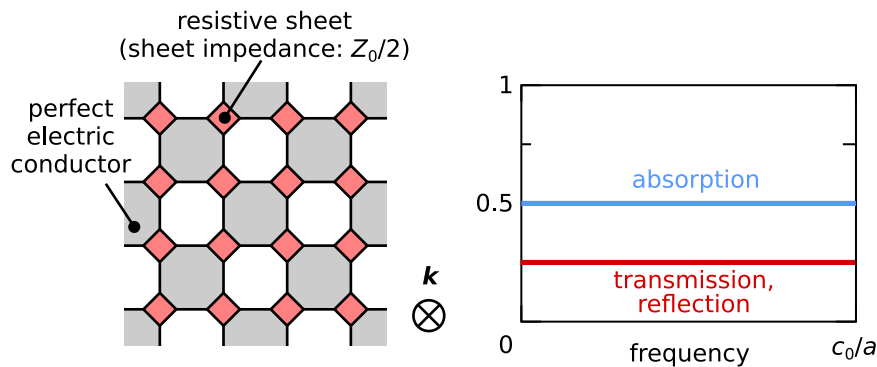


Figure 51. Resistive checkerboard-like metasurface, which is self-dual in terms of Babinet duality, and its power transmission, reflection, and absorption spectra.

The criticality of metallic checkerboard-like metasurfaces is utilized for dynamical metasurfaces to manipulate electromagnetic waves. By placing photoconductive materials like silicon or phase-change materials like vanadium dioxide (VO_2) between the metallic patches of checkerboard-like metasurfaces, researchers have realized optically tunable waveguides [99], capacitive–inductive switchable filters [50], dynamical polarizers [49], and dynamical switching of quarter-wavelength plates [52]. In addition to these experiments, dynamical planar-chirality switching is also theoretically proposed [51]. The advantage of these dynamical checkerboard-like metasurfaces is that we can achieve deep modulation of the electromagnetic characteristics of the metasurfaces because we dynamically induce phase transitions of the checkerboard-like metasurfaces.

6.3. Babinet Duality in Transmission-Line Models

Here, we consider Babinet duality in light of equivalent circuit models of metasurfaces. As discussed in Section 3, responses of metasurfaces can be described by equivalent circuit models. An electric metasurface in a vacuum can be modeled by an effective shunt impedance Z_{sh} inserted between two semi-infinite transmission lines with the characteristic impedance of Z_0 and the phase velocity of c_0 as shown in Figure 52. The complex amplitude transmission coefficient $\tau := \tilde{V}_t / \tilde{V}_{\text{in}}$ through the metasurface is written as

$$\tau = \frac{Z_{\text{sh}}}{Z_0/2 + Z_{\text{sh}}}. \quad (152)$$

On the other hand, for the dual problem with the complementary metasurface, the dual transmission coefficient τ^* is written as

$$\tau^* = \frac{Z_{\text{sh}}^*}{Z_0/2 + Z_{\text{sh}}^*}. \quad (153)$$

with the effective impedance of the dual metasurface Z_{sh}^* .

Requiring the same duality relation with Equation (144):

$$\tau + \tau^* = 1, \quad (154)$$

we obtain

$$Z_{\text{sh}} Z_{\text{sh}}^* = \left(\frac{Z_0}{2}\right)^2. \quad (155)$$

This equation indicates that the effective impedance of the complementary metasurface is given by the *dual* of the effective impedance of the original metasurface with respect to the reference impedance $Z_0/2$. In other words, the response of the complementary metasurface can be described by the dual circuit to the equivalent circuit of the original metasurface.

In particular, when the shunting equivalent circuit is a self-dual circuit like the bridge circuit shown in Figure 19, i.e., $Z_{\text{sh}} = Z_{\text{sh}}^* = Z_0/2$ (see Section 2.6), we have $\tau = \tau^* = 1/2$, and the transmission and reflection characteristics are frequency independent. Thus, we can connect the frequency-independent responses of self-dual resistive checkerboard-like metasurfaces to the constant resistance property of self-dual circuits.

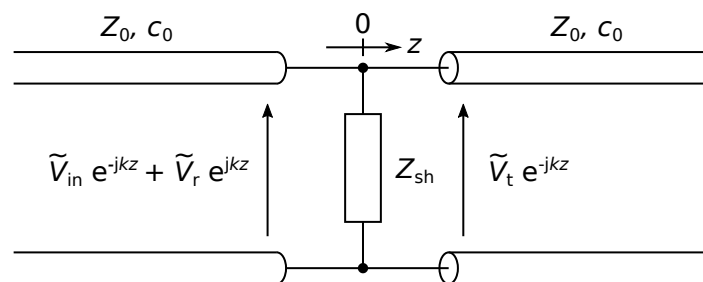


Figure 52. Transmission-line model for scattering of plane waves by an electric metasurface.

7. Conclusions

A space can be discretized with primary and dual meshes. Topological properties of the primary and dual meshes are related through Poincaré duality with each other. Especially in a $2n$ -dimensional space such as a plane ($n = 1$) and spacetime ($n = 2$), the dual counterpart of an inner-oriented n -chain is given by the outer-oriented n -chain. Thus, in an even-dimensional space, duality transformation does not alter the dimension of an n -chain; rather, it changes the characteristics of orientation for the chain. This special feature of even-dimensional spaces induces the complex structure for n -chains. Inner-oriented and outer-oriented objects work as real and imaginary parts of a complex

number, respectively. Due to this complex structure, the direction of an object is reversed when duality transformations are applied twice for the object. Electromagnetic duality is induced by a four-dimensional complex structure which appears from Poincaré duality. For a planar structure in the three-dimensional structure, Babinet duality holds due to the combination of electromagnetic duality and mirror symmetry. Keller–Dykhne duality is considered as an appearance of the Babinet duality at lower frequencies of direct current and alternating current. Circuit duality is interpreted as a discretized version of Keller–Dykhne duality.

Moreover, we can consider an additional invariance under duality transformation. When the system has such internal symmetry, it is called self-dual. The effective response of a self-dual system is automatically determined by the self-duality regardless of its components. This consequence of self-duality can lead to a frequency-independent input impedance and zero backscattering. Furthermore, critical response can even be predicted from self-duality, and it is leveraged to manipulate the spectra and polarization of electromagnetic waves.

In conclusion, we have unveiled the underlying geometrical structures behind various dualities in electromagnetic systems. Now, various dualities in electromagnetic systems emerge from the correspondence between quantities with two different kinds of orientations through Poincaré duality. The manifestations of self-duality in electromagnetic systems were consistently confirmed in a broad frequency range.

Author Contributions: Conceptualization, Y.N.; investigation, all authors; writing—original draft preparation, Y.N. (Sections 1, 2, 4, 5 and 7), Y.U. (Section 6), T.N. (Section 3); review and editing, all; visualization, all; project administration, Y.N.; funding acquisition, Y.N. and T.N.

Funding: This research was funded by a grant from the Murata Science Foundation, a grant from Shimadzu Science Foundation, and JSPS KAKENHI Grant Nos. 17K17777 and 17K05075.

Acknowledgments: The authors thank Shuhei Tamate for his interpretation of the algebraic treatment of circuits, Shogo Tanimura and Masao Kitano for their fruitful discussions on foundation of electromagnetism. Shin-itiro Goto and Jacob Koenig carefully read the manuscript and gave us valuable comments.

Conflicts of Interest: The authors declare no conflict of interest.

Appendix A. General Inner-Orientation Representation for Outer Orientation

The inner-orientation representation for outer orientation is generalized for any m -dimensional space. We use the fact that an inner orientation of a vector space U can be specified by a totally antisymmetric tensor $\omega : U \times U \times \cdots \times U \rightarrow \mathbb{R}$, which is linear for all input slots and satisfies $\omega(u_1, u_2, \cdots, u_i, \cdots, u_j, \cdots, u_i, \cdots, u_m) = -\omega(u_1, u_2, \cdots, u_j, \cdots, u_i, \cdots, u_m)$ for all possible $i \neq j$. For an inner-oriented vector space U , we select a positively-oriented basis (e_1, e_2, \cdots, e_m) and set ω satisfying $\omega(e_1, e_2, \cdots, e_m) = 1$. If $\omega(e'_1, e'_2, \cdots, e'_m) > 0$ is satisfied, a basis $(e'_1, e'_2, \cdots, e'_m)$ has the positive orientation. Reversely, for given $\omega \neq 0$, we can specify a basis (e_1, e_2, \cdots, e_m) with positive orientation as $\omega(e_1, e_2, \cdots, e_m) > 0$. Now, consider an outer-oriented linear subspace W in U with $l := \dim W < m := \dim U$. The surjective projection is denoted by $u \in U \mapsto [u] \in U/W$. Assume that an orientation of ambient space U is specified by a totally antisymmetric tensor with m slots ω_U and take a basis $([u_1], [u_2], \cdots, [u_{m-l}])$ which has positive orientation with respect to U/W . Then, we can define a totally antisymmetric tensor ω_W over W as

$$\omega_W(w_1, w_2, \cdots, w_l) := \omega_U(u_1, u_2, \cdots, u_{m-l}, w_1, w_2, \cdots, w_l), \quad (\text{A1})$$

where $w_1, w_2, \cdots, w_l \in W$ and the first $(m-l)$ -slots for the orientation tensor ω_U are contracted by an outer orientation. Thus, ω_W determines the inner orientation of W depending on the ambient-space orientation U . It is easily shown that the defined orientation of W does not depend on a specific choice of $u_1, u_2, \cdots, u_{m-l}$. The above discussion is applied to all tangent spaces smoothly, and then we can represent an outer-oriented cell as two inner-oriented cells.

Appendix B. Babinet's Principle for Transmission and Reflection Coefficients

We derive Babinet's principle for transmission and reflection coefficients for periodic screens (metasurfaces) in order to get insight into Babinet's principle under practical situations. We assume that the complex amplitude of the electric field of the incident plane wave in Figure 47a may be written as

$$\tilde{\mathbf{E}}_{\text{in}} = \tilde{E}_{\text{in}} \mathbf{e}_{\text{in}} \exp(-jkz), \quad (\text{A2})$$

where \mathbf{e}_{in} is a unit polarization vector perpendicular to \mathbf{e}_z . Here, \mathbf{e}_{in} can be a linear polarization like \mathbf{e}_x , \mathbf{e}_y or circular polarizations $\mathbf{e}_{\pm} := (\mathbf{e}_x \pm j\mathbf{e}_y)/\sqrt{2}$. Then, the scattered electric field can be expanded as

$$\tilde{\mathbf{E}}_{\text{s},\pm} = \left(\tilde{E}_{\text{s}} \mathbf{e}_{\text{in}} + \tilde{E}_{\text{s}}^{\perp} \mathbf{e}_{\text{in}}^{\perp} \right) \exp(\mp jkz) \quad (\text{A3})$$

in the far-field region, where $\mathbf{e}_{\text{in}}^{\perp}$ is the unit polarization vector orthogonal to \mathbf{e}_{in} . While in general all diffracted waves caused by the periodic screens should also be considered, we here focus on the zeroth order modes with the wavevector $\pm k\mathbf{e}_z$ for simplicity (for a more general formulation, see [37]). Thus, the complex amplitude transmission coefficients for the parallelly and orthogonally polarized modes τ and τ^{\perp} are given by

$$\tau := \frac{\tilde{E}_{\text{in}} + \tilde{E}_{\text{s}}}{\tilde{E}_{\text{in}}}, \quad (\text{A4})$$

$$\tau^{\perp} := \frac{\tilde{E}_{\text{s}}^{\perp}}{\tilde{E}_{\text{in}}}, \quad (\text{A5})$$

respectively. Similarly, we can write the complex amplitude reflection coefficients for the parallelly and orthogonally polarized modes ϱ and ϱ^{\perp} as

$$\varrho := \frac{\tilde{E}_{\text{s}}}{\tilde{E}_{\text{in}}} = \tau - 1, \quad (\text{A6})$$

$$\varrho^{\perp} := \frac{\tilde{E}_{\text{s}}^{\perp}}{\tilde{E}_{\text{in}}} = \tau^{\perp}, \quad (\text{A7})$$

respectively.

Next, we consider the dual problem shown in Figure 47b. Here, we fix the spatial orientation as $\sigma = \text{R}$ for simplicity, where R represents the right-hand system. As shown in Equation (141), the complex amplitude of the electric field of the dual incident wave is given by

$$\begin{aligned} \tilde{\mathbf{E}}_{\text{in}}^* &= Z_0(\tilde{\mathbf{H}}_{\text{in}})_{\text{R}} \\ &= \tilde{E}_{\text{in}}(\mathbf{e}_z \times \mathbf{e}_{\text{in}})_{\text{R}} \exp(-jkz) \\ &= \tilde{E}_{\text{in}} \mathbf{e}_{\text{in}}^* \exp(-jkz), \end{aligned} \quad (\text{A8})$$

where $\mathbf{e}_{\text{in}}^* := (\mathbf{e}_z \times \mathbf{e}_{\text{in}})_{\text{R}}$ is the dual incident polarization vector and $\tilde{\mathbf{H}}_{\text{in}} = Y_0 \mathbf{e}_z \times \tilde{\mathbf{E}}_{\text{in}}$ is used, which can be derived from Faraday's law. According to Equation (142), the totally reflected field is written as $\tilde{\mathbf{E}}_{\text{TR}}^* = -\tilde{E}_{\text{in}} \mathbf{e}_{\text{in}}^* \exp(jkz)$. From Babinet's principle, the dual scattered electric field is given by

$$\begin{aligned} \tilde{\mathbf{E}}_{\text{s},\pm}^* &= \mp Z_0(\tilde{\mathbf{H}}_{\text{s},\pm})_{\text{R}} \\ &= \mp Z_0(\pm Y_0 \mathbf{e}_z \times \tilde{\mathbf{E}}_{\text{s},\pm})_{\text{R}} \\ &= - \left[\tilde{E}_{\text{s}}(\mathbf{e}_z \times \mathbf{e}_{\text{in}})_{\text{R}} + \tilde{E}_{\text{s}}^{\perp}(\mathbf{e}_z \times \mathbf{e}_{\text{in}}^{\perp})_{\text{R}} \right] \exp(\mp jkz) \\ &= - \left(\tilde{E}_{\text{s}} \mathbf{e}_{\text{in}}^* + \tilde{E}_{\text{s}}^{\perp} \mathbf{e}_{\text{in}}^{\perp,*} \right) \exp(\mp jkz), \end{aligned} \quad (\text{A9})$$

where $e_{\text{in}}^{\perp,*} := (e_z \times e_{\text{in}}^{\perp})_{\text{R}}$ is the dual orthogonal polarization vector. Finally, the dual complex transmission and reflection coefficients can be expressed as

$$\tau^* := -\frac{\tilde{E}_{\text{s}}}{\tilde{E}_{\text{in}}}, \quad (\text{A10})$$

$$\tau^{\perp,*} := -\frac{\tilde{E}_{\text{s}}^{\perp}}{\tilde{E}_{\text{in}}}, \quad (\text{A11})$$

$$\varrho^* := -\frac{\tilde{E}_{\text{in}} + \tilde{E}_{\text{s}}}{\tilde{E}_{\text{in}}} = \tau^* - 1, \quad (\text{A12})$$

$$\varrho^{\perp,*} := -\frac{\tilde{E}_{\text{s}}^{\perp}}{\tilde{E}_{\text{in}}} = \tau^{\perp,*}. \quad (\text{A13})$$

Note that these coefficients are defined over the dual polarization basis e_{in}^* and $e_{\text{in}}^{\perp,*}$. If e_{in} is linearly polarized, then e_{in}^* corresponds to the orthogonal linear polarization. On the other hand, if e_{in} is circularly polarized, then $e_{\text{in}}^* = \pm j e_{\text{in}}$ and the dual polarization state is the same as the original one up to a phase factor $\pm j$, where $+$ ($-$) corresponds to the left (right) circular polarization. Here, we define handedness of circularly polarized plane waves from the receivers' side. This convention is commonly used in optics. By comparing Equations (A10) and (A11) with Equations (A4) and (A5), respectively, we finally obtain

$$\tau + \tau^* = 1, \quad (\text{A14})$$

$$\tau^{\perp} + \tau^{\perp,*} = 0. \quad (\text{A15})$$

Appendix C. Duality for Input Impedances of Antennas

We derive a dual relation for input impedances of antennas shown in Figure A1a,b. To simplify the discussion, we fix the spatial orientation as $\sigma = \text{R}$, where R represents the right hand. Two curves c_1 and c_2 on S are defined in Figure A1c. The total current along c_1 is calculated as

$$\tilde{I} = -2 \int_{c_2} (\tilde{\mathbf{H}}_+)_{\text{R}} \cdot d\mathbf{r}. \quad (\text{A16})$$

The electromotive force along c_1 is given by

$$\tilde{V} = \int_{c_1} \tilde{\mathbf{E}}_{\text{ext}} \cdot d\mathbf{r}. \quad (\text{A17})$$

For the dual antenna, we have a current along the c_2 direction as

$$\tilde{I}^* = \int_{c_1} \tilde{\mathbf{K}}_{\text{ext}}^* \cdot (e_z \times d\mathbf{r})_{\text{R}} = 2 \int_{c_1} Y_0 \tilde{\mathbf{E}}_{\text{ext}} \cdot d\mathbf{r} = 2Y_0 \tilde{V}. \quad (\text{A18})$$

On the other hand, the electromotive force along c_2 is given by

$$\tilde{V}^* = \int_{c_2} \tilde{\mathbf{E}}_+^* \cdot d\mathbf{r} = -Z_0 \int_{c_2} (\tilde{\mathbf{H}}_+)_{\text{R}} \cdot d\mathbf{r} = \frac{Z_0}{2} \tilde{I}. \quad (\text{A19})$$

Here, we introduce input impedances of antennas $Z_{\text{in}} = \tilde{V}/\tilde{I}$ and $Z_{\text{in}}^* = \tilde{V}^*/\tilde{I}^*$, where the real part of an antenna input impedance represents electromagnetic radiation as a loss. These input impedances satisfy

$$Z_{\text{in}} Z_{\text{in}}^* = \left(\frac{Z_0}{2} \right)^2. \quad (\text{A20})$$

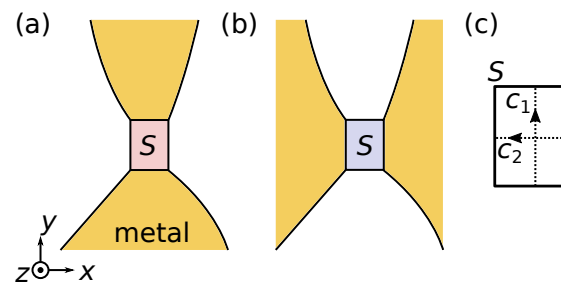


Figure A1. (a) antenna with a sheet admittance $Y_s(x, y)$ ($=: Z_s(x, y)^{-1}$) on $z = 0$ is connected to voltage source $\tilde{E}_{\text{ext}}(x, y)$, which is assumed to be in the y direction, on S ; (b) dual antenna with a sheet admittance $Y_s^*(x, y)$ ($=: Z_s^*(x, y)^{-1}$) satisfying Equation (137) on $z = 0$ is connected to current source $\tilde{K}_{\text{ext}}^*(x, y) = 2Y_0\Omega^\sigma e_z \times \tilde{E}_{\text{ext}}$ on S ; (c) definition of two curves on S .

References

1. Sykes, M.F.; Essam, J.W. Exact Critical Percolation Probabilities for Site and Bond Problems in Two Dimensions. *J. Math. Phys.* **1964**, *5*, 1117–1127. [[CrossRef](#)]
2. Russo, L. On the Critical Percolation Probabilities. *Z. Wahrscheinlichkeitstheorie Verw. Geb.* **1981**, *56*, 229–237. [[CrossRef](#)]
3. Kramers, H.A.; Wannier, G.H. Statistics of the Two-Dimensional Ferromagnet. Part I. *Phys. Rev.* **1941**, *60*, 252–262. [[CrossRef](#)]
4. Vilar, H.S.D. La Dualité en électrotechnique. *L'Eclairage Electrique* **1901**, *27*, 252–259.
5. Russell, A. *A Treatise on the Theory of Alternating Currents*, 2nd ed.; Cambridge University Press: Cambridge, UK, 1914.
6. Keller, J.B. A Theorem on the Conductivity of a Composite Medium. *J. Math. Phys.* **1964**, *5*, 548–549. [[CrossRef](#)]
7. Dykhne, A.M. Conductivity of a Two-dimensional Two-phase System. *Sov. Phys. JETP* **1971**, *32*, 63–65.
8. Mendelson, K.S. A theorem on the effective conductivity of a two-dimensional heterogeneous medium. *J. Appl. Phys.* **1975**, *46*, 4740–4741. [[CrossRef](#)]
9. Heaviside, O. On the Forces, Stresses, and Fluxes of Energy in the Electromagnetic Field. *Philos. Trans. R. Soc. Lond. A* **1892**, *183*, 423–480. [[CrossRef](#)]
10. Larmor, J. A Dynamical Theory of the Electric and Luminiferous Medium. Part III. Relations with Material Media. *Philos. Trans. R. Soc. A* **1897**, *190*, 205–493. [[CrossRef](#)]
11. Rainich, G.Y. Electrodynamics in the general relativity theory. *Trans. Am. Math. Soc.* **1925**, *27*, 106–136. [[CrossRef](#)]
12. Mushiake, Y. The Input Impedances of Slit Antennas. *J. IEE Jpn.* **1949**, *69*, 87–88.
13. Mushiake, Y. *Self-Complementary Antennas: Principle of Self-Complementarity for Constant Impedance*; Springer: London, UK, 1996.
14. Babinet, M. Mémoires d'optique météorologique. *Comptes Rendus de l'Académie des Sciences* **1837**, *4*, 638–648.
15. Copson, E.T. An integral-equation method of solving plane diffraction problems. *Proc. R. Soc. A* **1946**, *186*, 100–118. [[CrossRef](#)]
16. Meixner, J. Das Babinetsche Prinzip der Optik. *Z. Naturforschg.* **1946**, *1*, 496–498. [[CrossRef](#)]
17. Leontovich, M. On a theorem in the theory of diffraction and its application to diffraction by a narrow slit of arbitrary length. *JETP* **1946**, *16*, 474–479.
18. Booker, H.G. Slot aerials and their relation to complementary wire aerials (Babinet's principle). *J. Inst. Electr. Eng. Part IIIA Radiolocat.* **1946**, *93*, 620–626. [[CrossRef](#)]
19. Kotani, M.; Takahashi, H.; Kihara, T. On the leaking of electromagnetic waves. In *Recent Developments in the Measurement of Ultrashort Waves*; Korona: Tokyo, Japan, 1948; pp. 126–134. (In Japanese)
20. Meixner, V.J. Strenge Theorie der Beugung elektromagnetischer Wellen an der vollkommen leitenden Kreisscheibe. *Z. Naturforschg.* **1948**, *3a*, 506–518. [[CrossRef](#)]

21. Aoki, T. On the Diffraction of Electromagnetic Waves by Screens and Holes of Perfect Conductors (I) On a Dual Relation between the Diffractions of Electromagnetic Waves by Screens and that by Holes of Perfect Conductors. *J. Phys. Soc. Jpn.* **1949**, *4*, 183–185. [[CrossRef](#)]
22. Aoki, T. On the Diffraction of Electromagnetic Waves by Screens and Holes of Perfect Conductors (II) Approximate Formulas and their Applications. *J. Phys. Soc. Jpn.* **1949**, *4*, 186–191. [[CrossRef](#)]
23. Bouwkamp, C.J. Diffraction Theory. *Rep. Prog. Phys.* **1954**, *17*, 35–100. [[CrossRef](#)]
24. Neugebauer, H.E.J. Extension of Babinet's Principle to Absorbing and Transparent Materials, and Approximate Theory of Backscattering by Plane, Absorbing Disks. *J. Appl. Phys.* **1957**, *28*, 302–307. [[CrossRef](#)]
25. Baum, C.E.; Singaraju, B.K. Generalization of Babinet's Principle in Terms of the Combined Field to Include Impedance Loaded Aperture Antennas and Scatterers. In *Interaction Note No.217*; Air Force Weapons Lab.: Kirtland Air Force Base, NM, USA, 1974; pp. 1–53.
26. Moore, J. Extension of the Babinet principle to scatterers with lumped impedance loads. *Electron. Lett.* **1993**, *29*, 301–302. [[CrossRef](#)]
27. Solymar, L.; Shamonina, E. *Waves in Metamaterials*; Oxford University Press: New York, NY, USA, 2009.
28. Glybovski, S.B.; Tretyakov, S.A.; Belov, P.A.; Kivshar, Y.S.; Simovski, C.R. Metasurfaces: From microwaves to visible. *Phys. Rep.* **2016**, *634*, 1–72. [[CrossRef](#)]
29. Chen, H.T.; Taylor, A.J.; Yu, N. A review of metasurfaces: physics and applications. *Rep. Prog. Phys.* **2016**, *79*, 076401. [[CrossRef](#)] [[PubMed](#)]
30. He, Q.; Sun, S.; Xiao, S.; Zhou, L. High-Efficiency Metasurfaces: Principles, Realizations, and Applications. *Adv. Opt. Mater.* **2018**, *6*, 1800415. [[CrossRef](#)]
31. Engheta, N. Circuits with Light at Nanoscales: Optical Nanocircuits Inspired by Metamaterials. *Science* **2007**, *317*, 1698–1702. [[CrossRef](#)]
32. Falcone, F.; Lopetegui, T.; Laso, M.A.G.; Baena, J.D.; Bonache, J.; Beruete, M.; Marqués, R.; Martín, F.; Sorolla, M. Babinet principle applied to the design of metasurfaces and metamaterials. *Phys. Rev. Lett.* **2004**, *93*, 197401. [[CrossRef](#)]
33. Chen, H.T.; O'Hara, J.F.; Taylor, A.J.; Averitt, R.D.; Highstrete, C.; Lee, M.; Padilla, W.J. Complementary planar terahertz metamaterials. *Opt. Express* **2007**, *15*, 1084–1095. [[CrossRef](#)]
34. Zentgraf, T.; Meyrath, T.P.; Seidel, A.; Kaiser, S.; Giessen, H.; Rockstuhl, C.; Lederer, F. Babinet's principle for optical frequency metamaterials and nanoantennas. *Phys. Rev. B* **2007**, *76*, 033407. [[CrossRef](#)]
35. Al-Naib, I.A.I.; Jansen, C.; Koch, M. Applying the Babinet principle to asymmetric resonators. *Electron. Lett.* **2008**, *44*, 1228–1229. [[CrossRef](#)]
36. Baum, C.E.; Kritikos, H.N. (Eds.) *Electromagnetic Symmetry*; Taylor & Francis: Washington, DC, USA, 1995.
37. Nakata, Y.; Urade, Y.; Nakanishi, T.; Kitano, M. Plane-wave scattering by self-complementary metasurfaces in terms of electromagnetic duality and Babinet's principle. *Phys. Rev. B* **2013**, *88*, 205138. [[CrossRef](#)]
38. Urade, Y.; Nakata, Y.; Nakanishi, T.; Kitano, M. Frequency-Independent Response of Self-Complementary Checkerboard Screens. *Phys. Rev. Lett.* **2015**, *114*, 237401. [[CrossRef](#)] [[PubMed](#)]
39. Baena, J.D.; del Risco, J.P.; Slobozhanyuk, A.P.; Glybovski, S.B.; Belov, P.A. Self-complementary metasurfaces for linear-to-circular polarization conversion. *Phys. Rev. B* **2015**, *92*, 245413. [[CrossRef](#)]
40. Urade, Y.; Nakata, Y.; Nakanishi, T.; Kitano, M. Broadband and energy-concentrating terahertz coherent perfect absorber based on a self-complementary metasurface. *Opt. Lett.* **2016**, *41*, 4472–4475. [[CrossRef](#)] [[PubMed](#)]
41. Baena, J.D.; Glybovski, S.B.; del Risco, J.P.; Slobozhanyuk, A.P.; Belov, P.A. Broadband and Thin Linear-to-Circular Polarizers Based on Self-Complementary Zigzag Metasurfaces. *IEEE Trans. Antennas Propag.* **2017**, *65*, 4124–4133. [[CrossRef](#)]
42. Takano, K.; Tanaka, Y.; Moreno, G.; Chahadih, A.; Ghaddar, A.; Han, X.L.; Vaurette, F.; Nakata, Y.; Miyamaru, F.; Nakajima, M.; et al. Energy loss of terahertz electromagnetic waves by nano-sized connections in near-self-complementary metallic checkerboard patterns. *J. Appl. Phys.* **2017**, *122*, 063101. [[CrossRef](#)]
43. Compton, R.C.; Macfarlane, J.C.; Whitbourn, L.B.; Blanco, M.M.; McPhedran, R.C. Babinet's principle applied to ideal beam-splitters for submillimetre waves. *Opt. Acta* **1984**, *31*, 515–524. [[CrossRef](#)]
44. Kempa, K. Percolation effects in the checkerboard Babinet series of metamaterial structures. *Phys. Status Solidi RRL* **2010**, *4*, 218–220. [[CrossRef](#)]

45. Edmunds, J.D.; Hibbins, A.P.; Sambles, J.R.; Youngs, I.J. Resonantly inverted microwave transmissivity threshold of metal grids. *New J. Phys.* **2010**, *12*, 063007. [[CrossRef](#)]
46. Edmunds, J.D.; Taylor, M.C.; Hibbins, A.P.; Sambles, J.R.; Youngs, I.J. Babinet's principle and the band structure of surface waves on patterned metal arrays. *J. Appl. Phys.* **2010**, *107*, 103108. [[CrossRef](#)]
47. Takano, K.; Miyamaru, F.; Akiyama, K.; Miyazaki, H.; Takeda, M.W.; Abe, Y.; Tokuda, Y.; Ito, H.; Hangyo, M. Crossover from capacitive to inductive electromagnetic responses in near self-complementary metallic checkerboard patterns. *Opt. Express* **2014**, *22*, 24787–24795. [[CrossRef](#)] [[PubMed](#)]
48. Tremain, B.; Durrant, C.J.; Carter, I.E.; Hibbins, A.P.; Sambles, J.R. The Effect of Rotational Disorder on the Microwave Transmission of Checkerboard Metal Square Arrays. *Sci. Rep.* **2015**, *5*, 16608. [[CrossRef](#)] [[PubMed](#)]
49. Nakata, Y.; Urade, Y.; Okimura, K.; Nakanishi, T.; Miyamaru, F.; Takeda, M.W.; Kitano, M. Anisotropic Babinet-Invertible Metasurfaces to Realize Transmission-Reflection Switching for Orthogonal Polarizations of Light. *Phys. Rev. Appl.* **2016**, *6*, 044022. [[CrossRef](#)]
50. Urade, Y.; Nakata, Y.; Okimura, K.; Nakanishi, T.; Miyamaru, F.; Takeda, M.W.; Kitano, M. Dynamically Babinet-invertible metasurface: A capacitive-inductive reconfigurable filter for terahertz waves using vanadium-dioxide metal-insulator transition. *Opt. Express* **2016**, *24*, 4405–4410. [[CrossRef](#)] [[PubMed](#)]
51. Urade, Y.; Nakata, Y.; Nakanishi, T.; Kitano, M. Theoretical study on dynamical planar-chirality switching in checkerboard-like metasurfaces. *EPJ Appl. Metamat.* **2017**, *4*, 2. [[CrossRef](#)]
52. Nakata, Y.; Fukawa, K.; Nakanishi, T.; Urade, Y.; Okimura, K.; Miyamaru, F. Reconfigurable Terahertz Quarter-Wave Plate for Helicity Switching Based on Babinet Inversion of an Anisotropic Checkerboard Metasurface. *Phys. Rev. Appl.* **2019**, *11*, 044008. [[CrossRef](#)]
53. Fernandez-Corbaton, I.; Fruhnert, M.; Rockstuhl, C. Objects of Maximum Electromagnetic Chirality. *Phys. Rev. X* **2016**, *6*, 031013. [[CrossRef](#)]
54. Lindell, I.V.; Sihvola, A.; Ylä-Oijala, P.; Wallén, H. Zero Backscattering From Self-Dual Objects of Finite Size. *IEEE Trans. Antennas Propag.* **2009**, *57*, 2725–2731. [[CrossRef](#)]
55. Fernandez-Corbaton, I.; Zambrana-Puyalto, X.; Tischler, N.; Vidal, X.; Juan, M.L.; Molina-Terriza, G. Electromagnetic Duality Symmetry and Helicity Conservation for the Macroscopic Maxwell's Equations. *Phys. Rev. Lett.* **2013**, *111*, 060401. [[CrossRef](#)]
56. Fernandez-Corbaton, I.; Molina-Terriza, G. Role of duality symmetry in transformation optics. *Phys. Rev. B* **2013**, *88*, 085111. [[CrossRef](#)]
57. Fernandez-Corbaton, I. Forward and backward helicity scattering coefficients for systems with discrete rotational symmetry. *Opt. Express* **2013**, *21*, 29885–29893. [[CrossRef](#)] [[PubMed](#)]
58. Paal, E.; Umbleja, M. Note on homological modeling of the electric circuits. *J. Phys. Conf. Ser.* **2014**, *532*, 012022. [[CrossRef](#)]
59. Frankel, T. *The Geometry of Physics: An Introduction*, 3rd ed.; Cambridge University Press: Cambridge, UK, 2011.
60. Bamberg, P.; Sternberg, S. *A Course in Mathematics for Students of Physics 2*; Cambridge University Press: Cambridge, UK, 1990.
61. Roman, S. *Advanced Linear Algebra*; Graduate Texts in Mathematics; Springer: New York, NY, USA, 2008.
62. Bossavit, A. Discretization of Electromagnetic Problems: The "Generalized Finite Differences" Approach. In *Handbook of Numerical Analysis*; Ciarlet, P., Ed.; Elsevier: Amsterdam, The Netherlands, 2005; Volume 13, pp. 105–197.
63. Hatcher, A. *Algebraic Topology*; Cambridge University Press: Cambridge, UK, 2001.
64. Lin, P. A Topological Method of Generating Constant Resistance Networks. *IEEE Trans. Circuit Theory* **1967**, *14*, 172–179. [[CrossRef](#)]
65. Feynman, R.; Leighton, R.; Sands, M. *The Feynman Lectures on Physics, Vol. II*; Addison-Wesley Publishing Company: Boston, MA, USA, 1965.
66. Lindell, I.V.; Sihvola, A.H. Duality Transformation for Nonreciprocal and Nonsymmetric Transmission Lines. *IEEE Trans. Microw. Theory Tech.* **1997**, *45*, 129–131. [[CrossRef](#)]
67. Heaviside, O. Electromagnetic induction and its propagation. *Electrician* **1887**, *19*, 79–81.
68. Yu, N.; Capasso, F. Flat optics with designer metasurfaces. *Nat. Mater.* **2014**, *13*, 139–150. [[CrossRef](#)]
69. Yu, N.; Genevet, P.; Kats, M.A.; Aieta, F.; Tetienne, J.P.; Capasso, F.; Gaburro, Z. Light Propagation with Phase Discontinuities: Generalized Laws of Reflection and Refraction. *Science* **2011**, *334*, 333–337. [[CrossRef](#)]

70. Kang, M.; Feng, T.; Wang, H.T.; Li, J. Wave front engineering from an array of thin aperture antennas. *Opt. Express* **2012**, *20*, 15882–15890. [[CrossRef](#)]
71. Huang, L.; Chen, X.; Mühlenbernd, H.; Li, G.; Bai, B.; Tan, Q.; Jin, G.; Zentgraf, T.; Zhang, S. Dispersionless phase discontinuities for controlling light propagation. *Nano Lett.* **2012**, *12*, 5750–5755. [[CrossRef](#)]
72. Lin, D.; Fan, P.; Hasman, E.; Brongersma, M.L. Dielectric gradient metasurface optical elements. *Science* **2014**, *345*, 298–302. [[CrossRef](#)]
73. Pfeiffer, C.; Grbic, A. Metamaterial Huygens' Surfaces: Tailoring Wave Fronts with Reflectionless Sheets. *Phys. Rev. Lett.* **2013**, *110*, 197401. [[CrossRef](#)] [[PubMed](#)]
74. Kuester, E.F.; Mohamed, M.A.; Piket-May, M.; Holloway, C.L. Averaged transition conditions for electromagnetic fields at a metafilm. *IEEE Trans. Antennas Propag.* **2003**, *51*, 2641–2651. [[CrossRef](#)]
75. Selvanayagam, M.; Eleftheriades, G.V. Circuit Modeling of Huygens Surfaces. *IEEE Antennas Wirel. Propag. Lett.* **2013**, *12*, 1642–1645. [[CrossRef](#)]
76. Needham, T. *Visual Complex Analysis*; Oxford University Press: Oxford, UK, 1997.
77. Perrins, W.T.; McPhedran, R.C. Metamaterials and the homogenization of composite materials. *Metamaterials* **2010**, *4*, 24–31. [[CrossRef](#)]
78. Burke, W.L. *Applied Differential Geometry*; Cambridge University Press: Cambridge, UK, 1985.
79. Bossavit, A. Whitney forms: A class of finite elements for three-dimensional computations in electromagnetism. *IEE Proc. A* **1988**, *135*, 493–50. [[CrossRef](#)]
80. Tarhasaari, T.; Kettunen, L.; Bossavit, A. Some realizations of a discrete Hodge operator: A reinterpretation of finite element techniques. *IEEE Trans. Magn.* **1999**, *35*, 1494–1497. [[CrossRef](#)]
81. Bossavit, A. A uniform rationale for Whitney forms on various supporting shapes. *Math. Comput. Simul.* **2010**, *80*, 1567–1577. [[CrossRef](#)]
82. Tsukerman, I. Effective parameters of metamaterials: A rigorous homogenization theory via Whitney interpolation. *J. Opt. Soc. Am. B* **2011**, *28*, 577–586. [[CrossRef](#)]
83. Calkin, M.G. An Invariance Property of the Free Electromagnetic Field. *Am. J. Phys.* **1965**, *33*, 958–960. [[CrossRef](#)]
84. Deser, S.; Teitelboim, C. Duality transformations of Abelian and non-Abelian gauge fields. *Phys. Rev. D* **1976**, *13*, 1592–1597. [[CrossRef](#)]
85. Drummond, P.D. Dual symmetric Lagrangians and conservation laws. *Phys. Rev. A* **1999**, *60*, R3331–R3334. [[CrossRef](#)]
86. Cameron, R.P.; Barnett, S.M. Electric-magnetic symmetry and Noether's theorem. *New J. Phys.* **2012**, *14*, 123019. [[CrossRef](#)]
87. Barnett, S.M.; Cameron, R.P.; Yao, A.M. Duplex symmetry and its relation to the conservation of optical helicity. *Phys. Rev. A* **2012**, *86*, 013845. [[CrossRef](#)]
88. Bliokh, K.Y.; Bekshaev, A.Y.; Nori, F. Dual electromagnetism: Helicity, spin, momentum and angular momentum. *New J. Phys.* **2013**, *15*, 033026. [[CrossRef](#)]
89. Deschamps, G. Electromagnetics and Differential Forms. *Proc. IEEE* **1981**, *69*, 676–696. [[CrossRef](#)]
90. Hehl, F.W.; Obukhov, Y.N. *Foundations of Classical Electrodynamics: Charge, Flux, and Metric*; Birkhäuser: Boston, MA, USA, 2003.
91. Kitano, M. Reformulation of Electromagnetism with Differential Forms. In *Trends in Electromagnetism—From Fundamentals to Applications*; Barsan, V., Lungu, R.P., Eds.; IntechOpen: London, UK, 2012; Chapter 2, pp. 21–44.
92. Gratus, J. A pictorial introduction to differential geometry, leading to Maxwell's equations as three pictures. *arXiv* **2017**, arXiv:1709.08492.
93. Teixeira, F.L. Lattice Maxwell's Equations. *Prog. Electromagn. Res.* **2014**, *148*, 113–128. [[CrossRef](#)]
94. Jackson, J.D. *Classical Electrodynamics*, 3rd ed.; Wiley: New York, NY, USA, 1998.
95. Yeh, C. Boundary conditions in electromagnetics. *Phys. Rev. E* **1993**, *48*, 1426–1427. [[CrossRef](#)]
96. Singh, R.; Rockstuhl, C.; Menzel, C.; Meyrath, T.P.; He, M.; Giessen, H.; Lederer, F.; Zhang, W. Spiral-type terahertz antennas and the manifestation of the Mushiake principle. *Opt. Express* **2009**, *17*, 9971–9980. [[CrossRef](#)]
97. Ulrich, R. Far-infrared properties of metallic mesh and its complementary structure. *Infrared Phys.* **1967**, *7*, 37–55. [[CrossRef](#)]

98. Foster, R.M. A reactance theorem. *Bell Syst. Tech. J.* **1924**, *3*, 259–267. [[CrossRef](#)]
99. González-Ovejero, D.; Martini, E.; Loiseaux, B.; Tripon-Canseliet, C.; Mencagli, M.; Chazelas, J.; Maci, S. Basic Properties of Checkerboard Metasurfaces. *IEEE Antennas Wirel. Propag. Lett.* **2014**, *14*, 406–409. [[CrossRef](#)]



© 2019 by the authors. Licensee MDPI, Basel, Switzerland. This article is an open access article distributed under the terms and conditions of the Creative Commons Attribution (CC BY) license (<http://creativecommons.org/licenses/by/4.0/>).